NTNU

Norwegian University of
Science and Technology

Optimization and characterization of the Front Surface Field in Back-Contact Silicon Solar Cells

Egil Grøndal Krystad

Master of Science in Electronics

Submission date: July 2008

Supervisor: Bjørn-Ove Fimland, IET
Co-supervisor: Sean Erik Foss, IFE
Tor A. Fjeldly, UNIK

Norwegian University of Science and Technology
Department of Electronics and Telecommunications

Problem Description

This project will have the goal of fabricating a front surface field for optimal surface passivation to minimize minority charge carrier recombination at the front surface of a back-contacted interdigitated monocrystalline silicon solar cell. The work will consist of two parts: Simulation of the diffusion process and the subsequent electronic properties using the Silvaco software (Athena), and fabrication of test structures which are characterized with regard to resulting dopant profile and surface passivation. Correlation between simulation and measurement will be sought to obtain a thorough understanding of the process. For this, comparison of measured and simulated sheet resistances in n+ - p structures will be used to give an indication of correlation. Fabricated n+ - n structures will be used for measurements of surface passivation. This will be correlated with the simulated device perfomance.

Assignment given: 11. February 2008
Supervisor: Bjørn-Ove Fimland, IET

Abstract

Interdigitated back-contact (IBC) solar cells are devices requiring very high carrier lifetimes. In this thesis, an investigation of the front-surface field (FSF) concept for increasing the effective lifetime of so-called back-junction Si solar cells has been carried out.

Various levels of phosphorus doping have been introduced into n-type Si wafers for the creation of n^+-n junctions, and the resulting lifetime has been characterized using photoconductance measurements, in order to obtain an understanding of FSF-optimized process parameters. The in-diffusion of dopants is assessed through the consideration of resulting dopant profiles by means of sheet resistance measurements on phosphorus-diffused p-type Si wafers. Computer simulation tools have been utilized for calculation of the dopant profiles, as well as for investigating the dependence of the effective lifetime on the dopant profile.

The results of the study show that an in-diffused front surface field is efficient for passivation of this solar cell structure, provided a moderate or high degree of charge carrier recombination in the silicon surface. When a non-ideal homogeneity of dopants is assumed, the optimal sheet resistance is found to be mainly dependent on the dopant concentration, rather than the depth of in-diffused dopants. It is shown by means of software simulations that a relatively low level of diffusion is necessary for good passivation with a front surface field. The optimal range of sheet resistances is assessed based on the simulations, and coincides well with previously published studies within the field of back-junction solar cells.

Preface

This thesis is the submission for my Master's degree at the Norwegian University of Science and Technology, NTNU. The work has been carried out at the Institute for Energy Technology (IFE) at Kjeller during the spring of 2008. Experiments have been performed at the laboratory of the Solar Energy Department at the institute.

These months at IFE have been very valuable to me. I am thankful for being allowed to spend this period with the skilled and dedicated people at the Solar Energy Department. Thanks to Krister Mangersnes for introducing me to the Silvaco simulation tools. Countless late hours in the laboratory, especially with regard to the PECVD process, would have been much more difficult without the company and helping hand of Dr. Jeyanthinath Mayandi. I am also grateful to all the other employees at the Department, for willingly answering questions and helping me out with my requests.

In particular, I would like to express my gratitude to my supervisor here at IFE, Dr. Sean Erik Foss, with whom I have had many fruitful discussions during the process. Thank you for your motivating support!

Kjeller, 01.07.2008

Egil Krystad

Contents

List of Figures

Chapter 1

Introduction

Photovoltaic solar cells convert electromagnetic radiation into electrical power. This conversion was described as early as 1884 by Becquerel's photovoltaic theory. However, it was not until 1954 the first practically applicable solar cell was invented at Bell Laboraties [1]. Photovoltaics have since then been found useful within several fields. For example, as it is a light-weight source for energy, powered by sunlight, solar cell technology is very suitable for satellites and space stations. Because the utility aspect made the high cost bearable, solar arrays were used to power satellites as early as 1959 [2].

For terrestrial applications, conventional technologies of energy production have been dominating. However, due to more attention to the emissions of greenhouse gases combined with increasing costs of fossil energy sources, exploiting the energy from the sun is now by many considered as a significant contributor to energy supply in the future. In order to reach the point where photovoltaics may act as an energy source competitive with fossil, solar cell research strives to increase the power conversion efficiency. Partially helped by governmental funding and taxation on CO_2 emissions, solar electricity has now become a continuously growing segment of the energy industry in several parts of the world.

Fig. 1.1 shows the development through the recent years within installation of large-scale photovoltaic power plants worldwide, clearly reporting a large growth. The construction of plants in 2007 counts for a power output capacity of 490 MWp, which is more than the already installed capacity in 2006 [3]. This indicates that the capacity growth will continue to increase in the years to come.

As of this writing, the highest official energy conversion efficiency achieved in solar cell research is 40.7 % [4]. Commercially available solar cell modules yield significantly lower efficiencies. Among the most critical issues for a fur-

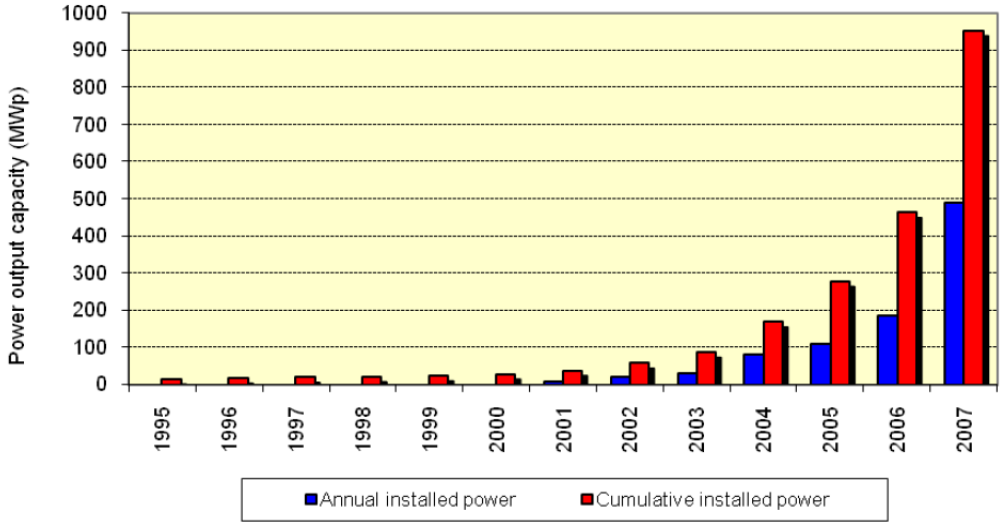

Figure 1.1: The annual and cumulative growth of installed large-scale solar cell power plants [3].

ther growth within photovoltaics are maximizing the achievable power per solar cell area, and minimizing the power cost. Obviously, finding the most advantageous technology for commercial application is a matter of compromise between these two issues.

In this thesis, one promising solar cell technology will be investigated. The concept of *interdigitated back-contact* (IBC) solar cells was first reported by Lammert and Schwartz [5] and has received much attention during recent years.

Chapter 2

Theory

The concept of photovoltaic solar cells is based on semiconductor physics. This chapter presents the theoretical background necessary to understand the following chapters.

2.1 Semiconductors

Photovoltaic energy generation is the conversion of energy from sunlight into electrical power based on excitation of charge carriers in semiconductors. In this section, the fundamental theory of semiconductors is listed and relevant quantities for describing semiconductor-based solar cells are introduced. The main litterature references used for this section are 'The physics of solar cells' by J. Nelson [6] and 'Solid state electronic devices' by B.G. Streetman and S.K. Banerjee [7].

2.1.1 Charge carriers in semiconductors

A semiconductor material exhibits an energy gap, or band gap, which divides two bands of possible electron energy states; the valence band and the conduction band. No possible states exist in the band gap of an ideal semiconductor crystal. At 0 K and with no incident illumination, the valence band is completely filled with electrons and the conduction band is filled with holes[1]. The material then acts as an insulator. The energy interval between the bands, known as E_g, varies in different semiconductors. For instance, the band gaps exhibited by silicon (Si), germanium (Ge) and gallium

[1] The presence of a hole implies absence of an electron, that is, there are no electrons in the conduction band when it is 'filled with holes'.

arsenide (GaAs) are 1.11 eV, 0.67 eV, and 1.43 eV, respectively.

In a *doped* semiconductor, available energy states are introduced in the band gap. Although several elements may be used for doping, the dopant energy level is different from element to element and it is advantageous to obtain dopant levels close to one of the band gap edges. Dopants normally introduced into silicon are phosphorus (P) for n-type doping and boron (B) or aluminum (Al) for p-type doping.

Illumination of a semiconductor may excite charge carriers across the full band gap energy. Photon energies larger than E_g will excite an electron across the band gap to the conduction band. Hence, the concentration of excess electrons in the conduction band is larger during illumination than in the dark. Excess electron concentration is also known as the *injection level* of charge carriers and is commonly denoted as Δn.

2.1.2 Carrier transport

The initial cause of electrical energy generation in a solar cell is the p-n junction; namely, a semiconductor material of a certain extension, of which one side is donor doped and the other side acceptor doped, commonly referred to as the n side and the p side, respectively. Due to diffusion, a small ratio of dopant-induced charge carriers of both polarities are positioned on their respective opposite sides across the junction and occupy available states on each side. The result is a charge depleted area, the depletion region, which is accompanied by an electric field due to the polarity difference, causing a drift force to act on the diffusing charge carriers. The depletion region will only extend over a certain length, since the carrier drift counters the effect of carrier diffusion.

Assume that an incoming photon, with a sufficiently high energy to excite a lattice atom and thus create an electron-hole pair ($h\nu > E_g$), strikes the semiconductor material near the p-n junction. The electric field created by the electrostatic potential across the junction causes a drift of free electrons towards the n-side, and an oppositely directed drift of free holes. Depending on the properties of the semiconductor and the quality of the semiconductor material, a certain number of the electron-hole pairs created from illumination reach the p-n junction. The junction serves to separate the hole and electron from each other. The carriers may be directed into an external circuit, contributing to a net current.

2.1.3 Fermi levels and band diagrams

In a semiconductor, the Fermi energy level (E_F) represents the energy state for which the probability of electron occupation equals $\frac{1}{2}$ under thermal equilibrium. The concept of Fermi levels allows for an easy analysis of semiconductor energies. For an undoped semiconductor, E_F lies in the middle of the band gap. The fermi level of an n-doped semiconductor is closer to the conduction band energy E_c than the valence band energy E_v, and vice versa for a p-doped semiconductor. Under thermal equilibrium, there can be no spatial variations in the Fermi level since there is no net charge transport. This can be used to combine the energy bands on the two sides of the junction in the case of no excess charge carriers; the Fermi level of the p-side will equal that of the n-side. In Figs. 2.1, or band diagram, of a p-n junction is shown.

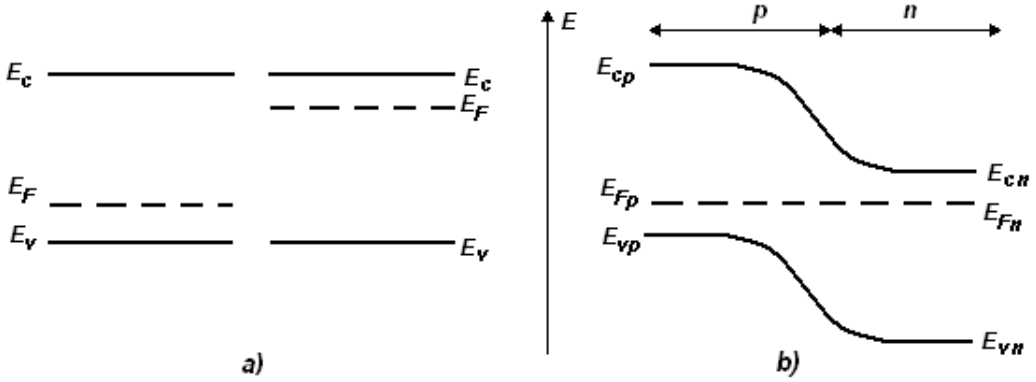

Figure 2.1: Schematic representation of a p-n junction and its Fermi levels. a) The n-side and the p-side separated from each other. b) The p-n junction at thermal equilibrium.

In the absence of thermal equilibrium, the principle of Fermi levels is not valid as excess carriers are present in addition to intrinsic charges. In this case an equivalent Fermi level is used, which includes the net effect from the presence of both fixed charges and excess charge carriers. The so-called quasi-Fermi levels F_n and F_p allow for a band diagram for the non-equilibrium situation.

2.1.4 Recombination

Photoexcited charge carriers have a certain probability of recombining, which means the electron loses the energy it has gained from the excitation and decays across the band gap to the valence band, filling the place of a hole. The extent of recombination depends on the number of impurities in the mate-

rial; both dopants and other impurities will cause recombination. Impurities or defects present in the crystal lattice may introduce possible energy states within the band gap, increasing the probability of recombination.

The charge carrier energy obviously decreases during recombination; additionally, in recombination processes involving phonons, there is also a change in carrier momentum. As is subsequently shown in section 2.2, the total recombination is a sum of different mechanisms, where several factors contribute to which mechanism is most significant [8].

The probability of recombination can be described using the quantity of recombination lifetime, τ, defined as $\tau = \Delta n/U$, where the quantity U, with denomination $\mathrm{cm}^{-3}\mathrm{s}^{-1}$, is the net recombination rate. Within the lifetime, charge carrier must be transported across the p-n junction in order to produce a net current; τ is therefore a very useful quantity in characterization of solar cells.

The nature of the recombination depends on the band gap properties. An *indirect* band gap transition involves a change in charge carrier momentum in addition to the energy change across the band gap. Silicon exhibits an indirect band gap. GaAs is an example of a *direct* band gap semiconductor, in which the recombination occurs with no change in momentum.

2.1.5 Silicon manufacture

Production of silicon for solar cells begins with SiO_2 (quartz), which occurs in large quantities in the Earth's crust. The quartz is reduced to silicon by means of heating in combination with carbon, resulting in metallurgical grade silicon. This material has a high concentration of impurities and is purified to yield polysilicon, for which there exists a range of technologies. In order to obtain monocrystalline silicon, which resembles a continuous crystal lattice with no grain boundaries, polysilicon may either be pulled from a melt using a seed crystal (the Czochralski method), or be subjected to an RF field which melts the polycrystalline rod locally multiple times (the Float-zone method). Silicon ingots of the desired purity and crystallography are then cut into wafers of the desired thickness. For applications within in the electronics industry, wafer thicknesses normally are in the region of 600-800 μm [9]. Photovoltaic applications often require thinner wafers.

2.2 Mechanisms of recombination

Several mechanisms contribute to determine the effective lifetime of a semiconductor crystal. In this section recombination is more closely investigated and the different contributions are specified.

2.2.1 Recombination contributions

There are three distinctive contributions to recombination in semiconductors [8]:

In *radiative* recombination, an excited electron decays to the valence band where it recombines with a hole, emitting a photon in the process. The energy of the released photon equals the band gap energy. This recombination is likely to occur if a photoexcited electron is not separated from the hole. For silicon and other indirect semiconductors, the radiative process also involves a change in momentum, as described above.

Band-to-band Auger recombination is a mechanism in which the excess energy from electron-hole recombination leads to the excitation of a third charge carrier instead of emission of a photon. The resulting charge carrier decays to its initial state and a phonon is generated.

Defect energy levels inside the band gap also cause recombination, and it is therefore desirable that a semiconductor for photovoltaic applications resembles an ideal crystal, as well as having a low concentration of unwanted impurities. Defects introduce energy states in the band gap, through which charge carriers may recombine. In the process of defect-level recombination a phonon is normally released, which results in heating of the material. The mechanism is described by the *Shockley-Read-Hall* (SRH) model, which, based on some simplifying assumptions, enables calculation of the recombination rate implied by one particular defect. The model involves a trap energy level E_t in the band gap, caused by the defect. An electron may decay from the conduction band to the defect level, and further to the valence band.

A resultant bulk lifetime can be found by summing up the inverse of the contribution from each lifetime mechanism,

$$\tau_b = \left(\frac{1}{\tau_{\text{rad}}} + \frac{1}{\tau_{\text{Auger}}} + \frac{1}{\tau_{\text{defect}}}\right)^{-1} \tag{2.1}$$

2.2.2 Surface recombination

The surface of a wafer is particularly prone to defects, due to the many unpaired valence electrons, so-called 'dangling bonds', as well as surface-affecting process steps (chemical residues). Recombination in the surface is therefore treated as a separate contribution to the defect-level recombination mechanism and is distinguished from the bulk lifetime contributions. The extent of surface recombination is addressed in terms of surface recombination velocity (SRV), defined as

$$S = \frac{U_s}{\Delta n_s} \tag{2.2}$$

where the *surface recombination rate* U_s here is measured in units of $cm^{-2}s^{-1}$ [8].

The lifetime components resulting from all contributions, including the surface recombination, add up to a total value referred to as the effective lifetime, τ_{eff}. As for the components of the bulk lifetime, contributions to lifetime are inversely added; thus the mechanism yielding the lowest lifetime contribution defines the maximum limit of effective lifetime:

$$\tau_{\text{eff}} = \left(\frac{1}{\tau_b} + \frac{1}{\tau_{\text{surface}}}\right)^{-1} \tag{2.3}$$

2.3 Dopant diffusion

In general, diffusion is the motion of some group of particles, which increases the degree of homogeneity in particle distribution. In doping of semiconductors, understanding the diffusion mechanisms of dopant atoms is important, for instance to monitor and optimize the dopant level inwards in the material or the abruptness of p-n junctions.

Several methods exist for introduction of dopants in semiconductors. In the IC (integrated circuits) industry, *ion implantation* has become the main choice. In a typical ion implant system, ions are accelerated from a gas containing the desired implant elements, and are guided by electrostatic deflection plates to be implanted at the desired position of the target wafer. The ion implant technology offers good selectivity and the dopant introduction is highly anisotropic, which is appropriate for the low dimensions in IC fabrication [9]. *In-diffusion* of dopants is the concept which has now been replaced with ion implantation for production of electronic circuits, but is highly suitable to photovoltaic applications.

This section first describes the theory of diffusion. Methods of in-diffusion are then treated, and finally the theory of dopant concentration with respect to wafer depth (the dopant profile) is considered.

2.3.1 Diffusion principles

There are several mechanisms by which an impurity atom may diffuse through a semiconductor material. Assume an impurity atom is placed in the crystal lattice. The atom may be placed either between lattice sites or at lattice sites; that is, it may be interstitially or substitionally located. Interstitial atoms diffuse significantly faster than substitonal atoms because energy is needed for an atom to occupy a lattice site. However, atoms in interstitial locations do not bond with the material lattice; therefore, unless energy (i.e. heat) is applied to the atoms enabling for movement into a substitional site, the diffusion does not affect conducting properties of the material. Substitional diffusion of impurities may be represented by two main mechanisms, direct exchange and vacancy exchange. The former mechanism involves two different atoms changing place, while the latter is the movement of an atom into a vacancy location, which requires less energy [10].

The ability for a certain atom to diffuse through solid-state matter is called diffusivity, measured in cm^2s^{-1}. Diffusivity is dependent on several properties, such as material density and occurences of impurities and crystal defects.

The diffusivity may be expressed by an Arrhenius relation as

$$D(T) = D^0 \exp(-\frac{E_A}{kT}) \tag{2.4}$$

where, in the ideal case, the prefactor D^0 and the activation energy E_A are constant for a given element diffusing in a given solid [10]. Hence, the diffusivity increases with temperature and decreases with activation energy.

2.3.2 Deposition of dopants

In several process steps within the semiconductor industry, a *spinner* is used for deposition of liquid substances. A circular wafer is placed on a vacuum chuck and a few ml of the liquid is applied onto the wafer center. The wafer is spun at large velocities (up to 5000 rpm , dependent on the desired resulting layer thickness). The process creates a uniform distribution of the liquid on the wafer [9].

In solar cell manufacture, however, the wafer size utilized is often large and the wafers used are commonly square rather than circular, to exploit the

available silicon material in terms of multiple-wafer installation into modules. Also, a critical issue within solar cell production for commercial application is the development of fast, effective production lines. In many cases, since establishment of a large-scale industrial production facility for solar cells involves vast investment costs, it is advantageous to avoid methods consisting of several separate process steps. In-line tools have therefore become common; for instance, conveyer belts are often utilized to transport wafers continuously through the various processes. In this context, spinning of a wafer would require a temporary halt in the process.

These requirements call for other methods for dopant application than the spin-on technique. Dopant in-diffusion involves application of diffusants to the wafer surface, followed by diffusion of the dopant atoms at high temperatures. A range of solar cell manufacturers utilize a process where the wafer surface prior to heating in a diffusion furnace is treated with a mist of dopant-containing liquid [11]. The diffusants may also be deposited during a CVD (chemical vapor deposition) process, as reactants contained in a gas which is introduced over the wafer surface.

2.3.3 Dopant profile

Dopants diffusing into a background-doped semiconductor will generally create a gradual p-n junction, although an abrupt transition between the n-side and the p-side would normally be desireable as an ideal case. The dopant concentration as a function of depth, commonly referred to as the dopant profile, depends on the diffusivity. For a given diffusion temperature, a large diffusivity yields a high level of in-diffusion and thus a deeper dopant profile.

For calculations of the relationship between profiles and the electronic properties, it is convenient to express the profile mathematically with respect to wafer depth. A common representation of the dopant profile can be calculated from Fick's diffusion laws, where some simplifying assumptions about the diffusion are made. Assuming an infinite source of diffusants directly above the semiconductor surface, the concentration versus the depth z and time t then shows a complementary error function dependence [10]:

$$C(z,t) = C_s \mathrm{erfc}\Big(\frac{z}{2\sqrt{Dt}}\Big), t > 0 \tag{2.5}$$

where C_s is the dopant concentration at the surface and $\sqrt{Dt}$ is the characteristic diffusion length.

2.4 Sheet resistance of doped layers

Because in-diffusion of dopants in a silicon wafer surface creates available energy states in the band gap, the conductivity increases with the level of doping. It also means that the electrical resistivity ρ of a doped semiconductor layer is dependent on the layer depth due to the inevitable doping gradient. It is therefore inconvenient to utilize resistivity to characterize a diffused wafer. The *sheet resistance* quantity is commonly used instead.

A rectangular wafer of length L, width w and thickness t has a resistance of

$$R = \frac{\rho L}{wt} \tag{2.6}$$

where ρ is the resistivity. If a current is conducted between two points on the wafer surface, the resistance will be higher if the wafer width w is reduced. Thus the resistance is also an inappropriate quantity. Instead, it is common to use the term of sheet resistance, R_s. This is the simplest means of characterizing the dopant profile of a diffused wafer [10]. R_s is related to the resistivity as

$$R_s = \frac{\rho}{t} \tag{2.7}$$

Comparing with the resistance expression yields

$$R = \frac{R_s L}{w} \tag{2.8}$$

The denomination of R_s is ohms; however, to avoid confusion, sheet resistance is commonly expressed in units of 'ohms per square', $\Omega/\square$.

2.5 Back-contact solar cells: An approach to enhanced efficiency

Several technologies have been suggested for enhancement of the achievable power per area in silicon solar cells. Interdigitated back-contact cells is a concept which has proven to be a potential competitor to the conventional cell type while also being appropriate for large-scale production. SunPower Corporation, California, has introduced solar cells of this type with a commercially achievable efficiency of 22.9 % [12]. This section first describes the

main components involved in traditional solar cells, and further introduces the back-contact concept.

2.5.1 Conventional solar cells

The most common solar cell design through the last few decades has by now become quite well-known. A blue silicon surface, monocrystalline or multicrystalline, and partially covered with thin metal fingers, is easily recognized as a solar cell. The process which results in this appearance, assuming a lightly doped p-type silicon wafer as the starting point, begins with doping the front of the wafer with n-type doping, thereby creating a p-n junction in close vicinity to the front surface. The in-diffused region in the front surface is generally referred to as the *emitter* in solar cell terminology.

Next, the surface is treated with a passivating layer, commonly silicon nitride with a hydrogen content; this is what causes the blue-coloured surface appearance. The hydrogen within the nitride layer serves to fulfill uncompleted atomic valences, so-called dangling bonds, thereby reducing the number of surface defects.

In the final part of the fabrication, the cell is metallized; that is, well-conducting metal fingers are placed on the surface and contact with the underlying silicon through the passivating layer is obtained through heat treatment (firing). Also, the whole area of the back side is covered with metal for thorough conduction of charge carriers to the rear contact. See Fig. 2.2.

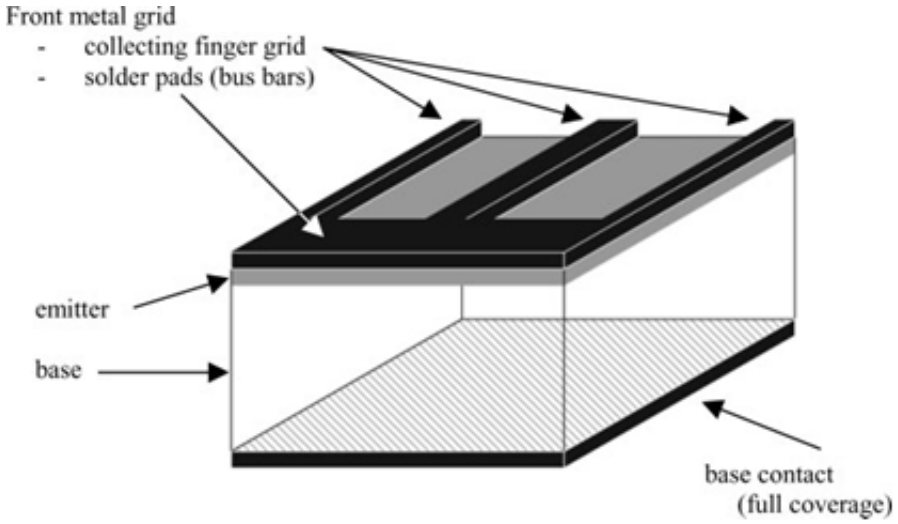

Figure 2.2: Schematic illustration of a conventional solar cell [13].

2.5.2 Back-contact solar cells

The idea of back-contact solar cells, first suggested in the mid-70's [5], is one of the contributions among several ideas for enhancing the solar cell efficiency beyond that of the conventional technology. The concept generally means removing metallization from the front surface of the cell. In order to collect electrons and holes at the respective electrodes, both contact polarities must then be available from the backside.

Several possible solutions have been suggested to achieve back-contacting, which can be divided into three distinct approaches: In metallization wrap-through (MWT) cells, the charge carriers arriving at the emitter fingers are conducted to the rear side with metal through bulk; hence the area-occupying busbars are removed from the front side and only the remaining fingers yield shading of incident solar radiation. In emitter wrap-through (EWT) cells, the emitter is extended by means of through-wafer connections to the rear side, beneath the metallization. Two p-n junctions are thus created, one at each side of the bulk region, which both collect photoexcited carriers [13]. The back-junction (BJ) approach, which is the technology applied by Sunpower Corp., involves rear placement of the emitter as well as the base, as shown in Fig. 2.3. Back-junction technology, being the concept investigated in the experimental work reported here, will be the back-contact cell technology in focus for the remainder of this thesis.

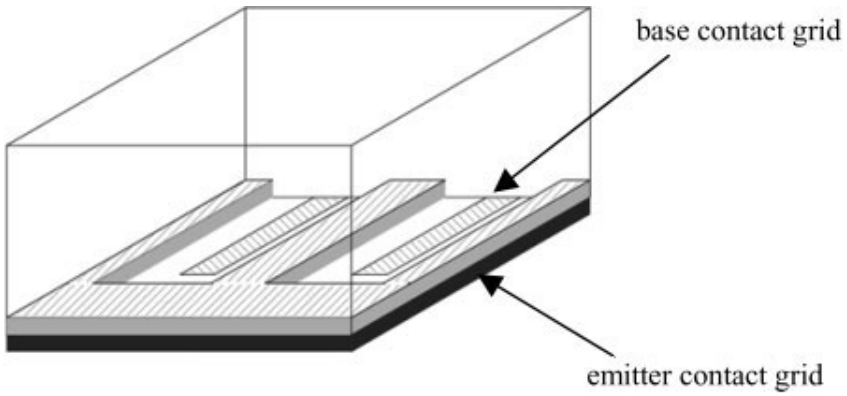

Figure 2.3: Schematic illustration of a back-junction solar cell [13].

When considering back-junction cells in comparison with conventional, there is an obvious advantage of reduced shading from metal fingers and busbars, which reflect approximately 10 % of the incoming light. Additional benefits arising from the back-contact solar cell concept are increased packing density of cells, since connections are limited to the rear side, and aesthetically that an unpatterned, non-metallized surface improves the visual appearance of

modules. Also, there is a potential for resistance reduction, since no explicit limitation to the thickness of metal fingers is present for back-contact cells [13].

2.6 Front surface passivation

Generally, passivation is enhancement of current from the incoming solar energy by reduction of recombination at defects and impurities. Oxide or nitride deposition on the silicon surface has been mentioned as a common means of passivation of the front surface and is more thoroughly treated in this section. Additional possible passivation techniques exist and are of importance for the back-junction concept.

2.6.1 Passivating thin films

In the surface of a semiconductor material, there is extensive disturbance in the lattice symmetry. Non-saturated atomic bonds establish available energy states, surface states, within the band gap. The concequence is a high level of recombination; in Eq. 2.2, this implies a high value of the surface recombination rate U_s and thus a high surface recombination velocity S [8].

Deposition of a silicon nitride (Si_xN_y) film on the surface is a good means of reducing the surface recombination. Silicon nitride has a high refractive index, and also has a good ability to saturate the dangling bonds at the surface. The most common manner of deposition the film is plasma-enhanced chemical vapor deposition (PECVD). The occurence of hydrogen in the nitride (coming from the ammonia used for deposition) is important for the degree of passivation; optimization of the Si_xN_y:H compound is therefore an important factor.

Recently, there has also been a significant focus on utilization of amorphous silicon for passivation. Studies have shown that deposition of hydrogenated a-Si as passivating film yields very low surface recombination velocities [14].

2.6.2 Front surface field

Similarly as for conventional cells, most of the charge carriers in a back-junction solar cell are generated near the surface. As both contact polarities in this case are placed on the back side, however, carriers must travel through the full bulk width to reach the interdigitated p-n junctions; this implies that a large bulk carrier lifetime is necessary.

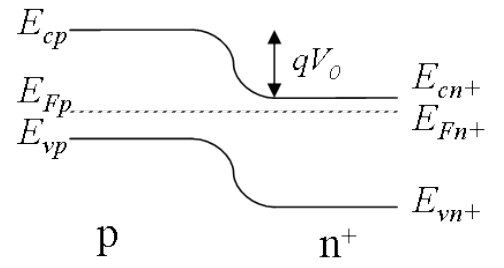

(a) p-n^+ junction

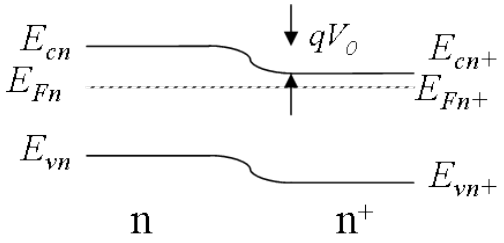

(b) n^+-n juntion

Figure 2.4: Band diagram of a p-n^+ junction and an n^+-n juntion, showing the valence (VB) and conduction (CB) bands and the Fermi levels. The built-in electrostatic potential, V_0, is higher in the case of a p-n junction.

Research into back-junction cells has shown that an electric field in proximity of the front surface is necessary for a sufficient carrier transport. Such a field may be introduced by creating a doping gradient (high-low junction) from the front surface and inwards in the cell. The band diagrams of a p-n^+ junction and an n^+-n juntion are shown in Figs. 2.4.

In a conventional solar cells with p-type bulk material, a similar high-low (p^+-p or n^+-n) junction is commonly used on the rear side, then called a back-surface field or BSF[2]. Exhibiting the same polarity as the bulk silicon but with a higher level of doping, the in-diffused region introduces a potential barrier which is low compared to that of a p-n junction; a built-in electric field is established, which transports photoexcited minority carriers downwards from the surface. The front and back surface fields hence serve to decrease the SRV value of the respective cell side.

The importance of a front surface field in a back junction solar cell was investigated by simulations in 2007 by Granek [15]. Here it was found that the extent of carrier transport necessary for the efficiency of a BJ solar cell to exceed 20 % can not be achieved without a front surface field. Furthermore,

[2]Aluminium, when used as backside metallization on p-type substrate solar cells, serves both as acceptor dopant for establishing a BSF, and as contact metal.

the results showed that when a front surface field is present, high efficiencies can be reached even with an imperfectly passivation of the BJ solar cell surface.

Chapter 3

Experimental

The purpose of the experimental work was to get an understanding of front-surface field with respect to the dopant profile. Monocrystalline wafers were cut into smaller pieces, henceforth referred to as the *samples* of the experiments. The work that was carried out consisted of two main parts, which both involved processing of a series of phosphorus-diffused Si wafers at different temperatures. Samples with p-type background doping were used to investigate the dopant profiles based on sheet resistance measurements. Samples with n-type background doping were then treated with the same process to enable measurements of the effective lifetime. This chapter will describe the processes used for fabrication and characterization of samples.

3.1 Experimental procedure

The main steps in the experimental work were

- In-diffusion of phosphorus in p-type samples for the formation of p-n junctions. This step was carried out to investigate two issues: The degree of homogeneity in phosphorus doping, and the dopant profiles resulting from the diffusion process.

- Measuring sheet resistance of the in-diffused p-type samples. As will be seen, the sheet resistance was examined using two different methods.

- In-diffusion of phosphorus to make n^+-n-n^+ structures. In order to obtain good passivation, phosphorus was diffused into both sides of each n-type sample. Subsequently the samples were treated with a passivating layer (a-Si).

- Measuring the effective lifetimes of diffused n-type samples.

3.2 Process steps in experiments

The processes carried out in the laboratory for deposition and in-diffusion of dopants are described in this section. The procedure and purpose of each process are explained. For a thorough description of the experimental procedure, see the 'Experimental details' section (3.4).

3.2.1 Dopant spray-on source

There are several reasons to avoid spinning of dopants in fabrication of solar cells, described in section 2.3.2. At the time of the present experimental work, the method used at IFE for dopant deposition (boron and phosphorus) was liquid spray-on, implemented in a setup designed and realized by the solar energy department, called 'Sprutus'. A schematical presentation of the Sprutus setup is shown in Fig. 3.1. In contrast to the spin-on method, spray-on application of diffusants offers in-line production possibilities, as it can be a part of the conveyer belt processing steps (section 2.3.2).

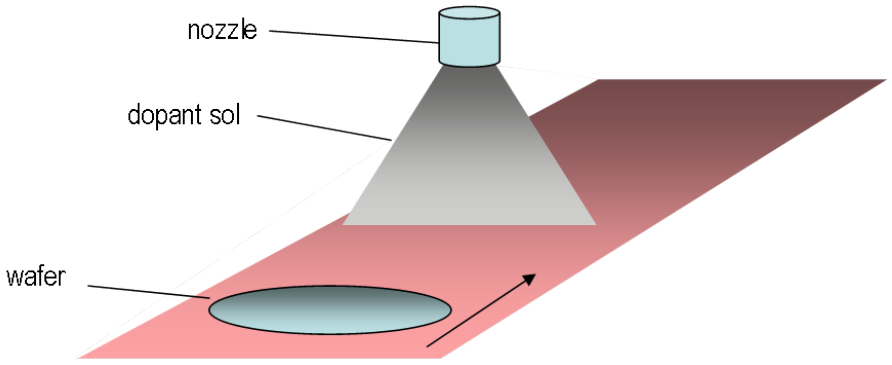

Figure 3.1: Schemactic of the 'Sprutus' dopant spray-on setup.

3.2.2 Sol-gel silicon dioxide

The liquid used for in-diffusion of phosphorus from the Sprutus apparatus is called a *sol*. The liquid is manufactured by Filmtronics, Inc., under the name P509. This matter exhibits gel-like properties, which means the viscosity increases when the deposited layer is subject to heat (baking). During the so-called sol-gel transition, the sol becomes rigid and porous. The transition

results in a SiO_2-similar oxide layer on the surface [16], from which the phosphorus atoms are diffused into the silicon during application of sufficiently high temperatures.

3.2.3 Baking and in-diffusion

Samples with a deposited phosphorus layer were placed in a temperature of 200 °C for 10 minutes for the sol-gel transition to take place. In-diffusion of the phosphorus was then done with heat treatment in an IR-heated furnace. The time of diffusion and temperatures utilized are described in section 3.4.

3.2.4 Oxide etch and oxidation

Native oxides from the ambient are unwanted in many process steps. An oxide layer introduces contamination into the crystal and gives poor electrical conduction to the contact metal. Wet etch using hydrofluoric acid is a common manner of removing an oxide layer from a silicon surface.

Removal of a silicon dioxide layer can in many cases not be done solely by a single dip in HF acid. For large oxide thicknesses, it is necessary to oxidize the deposited surface by means of a short period heat treatment at a high temperature in an oxygen-containing ambient, followed by another HF dip. This is more efficient because the new oxide layer grows into the wafer by consuming the existing silicon. The oxygen must travel through the oxide film to reach the silicon surface, but already after a short period of oxidation the new oxide layer separates the wafer surface from the deposited glass [8]. A HF dip treatment after the oxidation step will therefore etch the heat-induced oxide layer, removing the glass layer with it as well.

To be suitable for nitride or a-Si deposition for surface passivation, the wafer is subjected to additional cleaning using a piranha mixture, a strong solution that is a combination of H_2SO_4 and H_2O_2. The solution removes organic and metallic impurities.

3.2.5 Surface passivation and tempering

Application of the passivating layer was done using plasma-enhanced chemical vapor deposition (PECVD). Amorphous silicon (a-Si) was used, being the most satisfying method used for the plasma chamber at IFE at the time of the experiments. The wafer was then subjected to application of a temperature of 450 °C for a short duration (tempering), in order to couple the amorphous silicon with dangling bonds in the silicon surface.

3.3 Characterization methods

One of the most useful techniques for characterizing a complete solar cell is the illuminated current-voltage (I-V) curve, which may be achieved by illumination from a solar simulator lamp, a varying voltage bias applied across the cell contacts, and measurements of the resulting current. The IV curve of a well-passivated solar cell with small leak currents exhibits a high current-voltage product, that is, a high output power.

In the silicon wafer samples without metallization used in this work, however, no contacts conduct the photoexcited charge carriers out of the cell, meaning that the material properties must be investigated using other techniques. It is described in section 2.4, and will be shown in more detail in this section, that the dopant profile inwards from the wafer surface is closely related to the sheet resistance. Also explained is the characterization of a front surface field from effective lifetime measurements, and in which manner the lifetime has been measured in this work.

3.3.1 Measuring sheet resistance: Four-point probe

Four-point probing is a simple method for measuring the sheet resistance of a diffused semiconductor sample. The most common setup, and the one used in this work, is a collinear set of probes, of which a current is passed between the two outer ones. A voltmeter measures the current-induced voltage drop between the two inner probes, allowing for calculation of the sheet resistance based on the voltage-current ratio, as shown schematically in Fig. 3.2. Although the correction factor necessary to obtain the sheet resistance depends on the probe geometry and spacing between probes, it can be approximated as $R_{\mathrm{sh}} = 4.53 \times R_{\mathrm{eff}}$, where R_{eff} is the effective voltage-current ratio, when the spacing between probes is much larger than the junction depth [10].

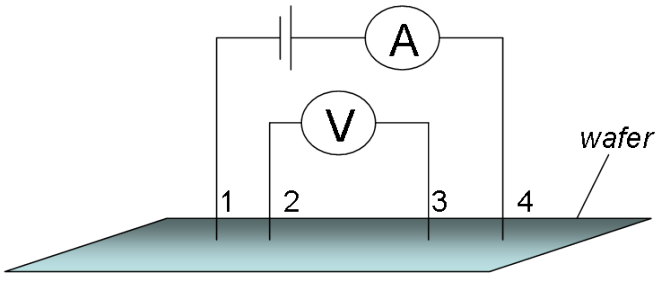

Figure 3.2: Schematic of a collinear-type four-point probe (based on [10]).

A batch of p-type wafers were processed to investigate the sheet resistance although n-type wafers were used for the final investigation of the lifetime

induced by the front surface field. The resulting junction from phosphorus in-diffusion in an n-type wafer is inappropriate for sheet resistivity measurements, because the p-n junction, which is formed when phosphorus is diffused into silicon with p-type background doping, must be present in order to characterize the dopant profile by means of four-point probing. This can be explained by considering the mechanisms distinct for this type of junction. The potential barrier across the p-n junction, and the consequent built-in electric field, prevents charge carriers from diffusing across the junction. Similarly, in-diffusion of donors in n-type material gives rise to a potential difference across a so-called n^+-n junction, considered in section 2.6.2; however, the magnitude of the n^+-n-junction field is significantly lower, allowing for charge carriers to move across it easily. This is seen on Fig. 2.4 in the theory chapter. Consequently, the current conducted during four-point probing may be expected to go some distance into the wafer and even across the high-low junction. Calculation of the sheet resistance based on the voltage-current ratio will therefore, in this case, be larger than the actual value. In four-point probing of a p-n junction, majority charges are repelled by the potential barrier and thus current is likely to flow in close proximity to the surface.

3.3.2 Mapping of sheet resistance: Semilab SHR

The Semilab WT-2000 is an apparatus which may, among other functions, be used to obtain a map of the sheet resistance of a diffused wafer surface. The measurement is made based on the voltage potential present on the wafer surface during illumination from a LED lamp. The front surface voltage potential resulting from the illumination is found using two capacitive sensors. The sheet resistance is related to this voltage potential, and is calculated by the software for each point measured on the wafer.

In the present work, Semilab mappings were conducted on some of the samples from each batch of in-diffused Si samples. The mapping is a very useful result as it gives an indication of the sheet resistance homogeneity across the wafer area. However, due to uncertainties in the calibration of the Semilab SHR, the four-point probe was chosen as the method for measurements of R_s. This is explained in more detail in section 5.1.1.

3.3.3 Measuring lifetime: Sinton WCT-100

In section 2.2, the concept of bulk lifetime was described, as well as the surface recombination mechanism. These contributions together yield the effective lifetime, which is a very valuable quantity in characterization of

the wafer material and optimization of process steps in the production of photovoltaics.

Several techniques exist and are in use for lifetime characterization. One example is the photoconductance decay method, in which the photoconductance is continuously measured during and after flash illumination. Since a higher lifetime yields conduction for a longer time after the flash, the slope of the decay (conductace vs time) gives information about the lifetime.

Effective lifetime may also be investigated with a method called quasi-steady-state photoconductance (qssPC). It is based on the assumption that excess carriers are close to steady-state, although the illumination source is a flash lamp. Hence the decay of the flash must be long for this method to be valid. The average excess carrier density, Δn_{av}, may be used to express the photogeneration current density J_{ph}, given by

$$J_{ph} = \frac{\Delta n_{av} q W}{\tau_{\mathrm{eff}}} \tag{3.1}$$

where W is the wafer thickness and q the electronic charge [17]. The excess photoconductance, σ_L, may also be expressed in terms of Δn, for given values of the electron and hole mobilities, μ_n and μ_p,

$$\sigma_L = q \Delta n_{av} (\mu_n + \mu_p) W \tag{3.2}$$

Combining the two expressions yields a photogeneration-dependence of the effective lifetime:

$$\tau_{\mathrm{eff}} = \frac{\sigma_L}{J_{ph}(\mu_n + \mu_p)} \tag{3.3}$$

The WCT-100 lifetime measurement apparatus, produced by Sinton Consulting Inc., exploits Eq. 3.3 by use of a flash lamp as described above. The photoconductance is found by means of a coil positioned underneath the wafer. Prior to conducting the flash and decay measurement, the WCT-100 must be calibrated with a reference sample. This way the correct relation is established between the incident light and the resulting lifetime. A photocell monitors the light intensity in proximity of the wafer position. For each point of measurement, the illumination is then known as well as the photoconductance and hence the lifetime can be calculated. Since the level of photoexcitation varies during the flash, one obtains the effective lifetime for a range of excess carrier concentrations. Constant illumination leads to an increased intrinsic carrier concentration, which in turn yields higher re-

combination [18]. Therefore, flash illumination is a convenient feature for both lifetime measurement methods described.

The quasi-steady state method takes the presumption that the rate of generation is approximately equal to the recombination. This means that the flash decay should not be too short. Low-quality or poorly passivated silicon exhibits a high level of recombination; therefore, a sufficiently high lifetime is necessary for a correct analysis and is a condition which must be satisfied for the QssPC technique [17].

3.4 Experimental details

In-diffusion of phosphorus on p-type wafers was done in the first part of the work, in order to characterize the dopant profiles with the use of sheet resistance measurements. In the next part, the same procedure and equal process parameters were used on n-type wafers, to find the relation between dopant profiles and the effective lifetime. Characterization of the samples consisted of sheet-resistance measurements of p-type samples and lifetime measurements of n-type samples. This section lists the details of the work.

3.4.1 Sample in-diffusion procedure

The p-type and n-type Si wafers were cut into smaller samples, listed in detail in table 3.1. Processing of samples began with native-oxide removal through etch in diluted hydrofluoric acid (5 % HF) for 2 minutes, followed by a 1-minute rinse in deionized (DI) water. Next, the wafers were sprayed with phosphorus using the Sprutus apparatus and baked at 200 °C for 10 minutes. The n-type wafers for lifetime measurements were treated with phosphorus spray on both sides, with a subsequent drying process for each spraying. Diffusion was then carried out in dry air ambient in a RTC-1210 belt furnace. In-diffusion of the n-type wafers was done at a constant diffusion duration of 25 minutes, while two durations were chosen for the p-type wafers; 25 minutes and 37.5 minutes. Most of the resulting phosphorus-containing glass layer was then removed in a 10-minute 5 % HF-dip. However, a subsequent oxidation was necessary to remove the remnants of the glass. This was achieved by heating in the belt furnace for 15 minutes at 800 °C in dry air, followed by a 5 % HF dip for 5 minutes to completely remove the glass layer.

	p-type samples	n-type samples
Geometry of origin wafers	Square, 156×156	Circular, d =100 mm
Geometry of sample	Square, 60×60	Quarter-circle
Surface	Unpolished	Polished
Characterization parameter	Sheet resistance	Effective lifetime
Characterization method	Four-point probe	Sinton WCT-100

Table 3.1: Details of the samples used.

3.4.2 Optimization of experimental conditions

Measures were taken to ensure as similar conditions as possible for each experiment and a low degree of unwanted impurities from the ambient. The P509 solution was stored in a refrigerator and had to be placed in room temperature some hours before spraying. To avoid clogging of the dopant spray nozzle, cleaning or brushing of the nozzle was done before using the Sprutus apparatus. Also, the time used between the processes of spraying and drying a wafer was critical due to the impact of airborne impurities which would easily stick to the phosphorus spray layer. The level of impurities in the laboratory imposed a significant risk of contamination and must be considered a contribution to variations in sample results.

The Sprutus apparatus allows for adjustment of several parameters concerning the spray-on process. In order to ensure good performance of the spray, an optimization of some of the parameters was carried out. Polished monocrystalline wafer samples were subjected to spraying, baking and diffusion. The number of spraying repetitions was varied: samples were sprayed either one, two or four times to investigate possible consequences of a thicker glass layer. The pressure of air and liquid was also varied due to a visibly unsatisfactory spraying performance in the initial phase.

Another important aspect is the concentration of the deposited P509 sol. Mainly being intended for spin-on purposes, the viscousity of the P509 phosphorus compound is rather high. Obviously, this is to have a uniform dispersion of sol over the wafer surface whilst maintaining the sol layer sufficiently thick when the wafer is spun. For the spraying method, however, the solution must be diluted in order to pass through the nozzle properly. There is reason to expect that the solution needs to form small droplets to have a homogeneous deposition. Experience with the Sprutus apparatus as well as hand-spraying experiments at IFE, has resulted in an ethanol-dilution of P509 in the ratio 1 to 4 currently being used. Two other concentration ratios were attempted utilized, to investigate the possibility of altering the phosphorus concentration in the deposited glass layer.

A characterization of the parameter variations was done by means of Semilab mappings of the sheet resistance to examine the homogeneity of the sprayed layer. The results are briefly presented in the Results chapter.

Chapter 4

Simulations

The investigation of dopant profiles was best conducted with the help of software simulations. To be able to compare the samples from experiments and simulations, however, it was necessary that the simulation resulted in a similar dopant profile as the samples resulting from in-diffusion for a given set of process parameters. For this, parameters for the in-diffusion of phosphorus was varied through simulations, aiming to obtain equal results for equal diffusion temperature and diffusion time. Dopant profile simulations are described in section 4.1. It was sought to utilize the resulting profiles as a basis for lifetime simulations, presented in section 4.2.

4.1 Simulations of dopant profile

Simulations of the effective lifetime were based on the dopant profiles exhibited by the samples processed. It was therefore necessary to find a representation of the dopant profile resulting from a given diffusion time and temperature. For this, the program Athena within the Silvaco software package was utilized. Athena is a tool for simulation of semiconductor structures which uses the finite element analysis method. Generally spoken the simulator is physically based, which means that physical relations and equations, to a certain level of complexity, have been implemented for finding semiconductor structures and their properties. With input material characteristics and process parameters given, the Athena simulator computes the resulting structure along with output values such as dopant concentration and sheet resistance.

Another possible solution for the determination of dopant profiles could be to utilize SIMS (secondary ion mass spectroscopy) technology, which is a widely

used method where the wafer is bombarded with a high-energy ion source, thus sputtering the wafer for some distance into the material, followed by mass spectroscopy. The method enables determination of impurity concentrations. However, for several reasons a SIMS process would be inconvenient for the experiment. It was desirable to retain an intact wafer surface for subsequent a-Si passivation and characterization; in addition, for the simulations of lifetime, reliable dopant concentrations for a range of depths inwards into the material must be provided. As will be shown later, simulations using the Athena software allow for determination of the dopant profile.

4.1.1 Tuning of diffusion parameters

The exact case of diffusion into silicon from a sprayed-on phosphorus layer is not supported in the Athena package. The diffusion was therefore approximated by using an oxide layer (SiO_2) model and implementing a phosphorus concentration into the simulated oxide. However, the in-diffusion will then differ somewhat from the real laboratory case. In the Appendix (Fig. 2) the data sheet for spin-on dopants from Filmtronics Inc. is shown. The initial concentration of oxide in the sol is only 5 %. To a certain extent, additional oxide is created due to oxygen which reacts with the silicon surface; however, this extent is difficult to predict. The diffusion of phosphorus atoms through the spray-on layer is inconsistent with simulations of an ordinary oxide layer (5.3.2). To obtain a more accurate model, the parameters of phosphorus diffusion in the oxide must be altered.

For the P509 sol, the concentration of phosphorus is 10.5 %, also described in the data sheet. It was necessary to find an approximate value for the phosphorus concentration for simulations of the diffusion process in Athena. Since the conditions of the sol-gel transition are difficult to describe physically, the relation between phosphorus concentration in the sol prior to baking and atomic phosphorus concentration after baking was uncertain. According to the manufacturer, a phosphorus concentration of 1×10^{21} cm^{-3} could be assumed in the undiluted sol [19]. The liquid was diluted with ethanol prior to spraying, of which a certain ratio must be expected to evaporate. This means that the effective concentration directly above the silicon surface is in the range 2×10^{20}-1×10^{21} cm^{-3}.

The chosen output parameter for reference between the lab results and the simulations was the sheet resistance R_s; that is, diffusivity in oxide was varied until R_s was equal in experiments and simulations for equal diffusion times and temperatures. See Fig. 4.1.

The Arrhenius relation for the diffusivity, Eq. 2.4, contains two lattice-dependent coefficients; a prefactor D^0 and the activation energy E_A. It was

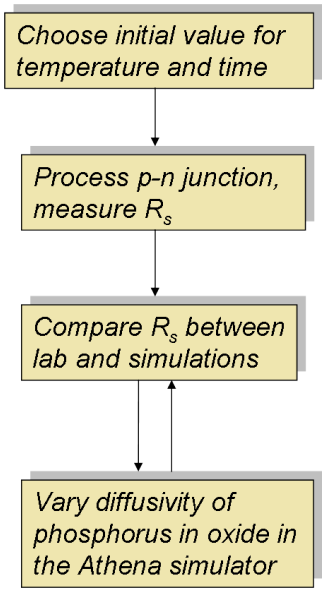

Figure 4.1: Schematic of the procedure which was carried out to correlate simulations with lab results.

convenient to find several combinations of the coefficients which all yielded the same diffusivity for a give temperature, thus obtaining different curves for R_s versus temperature by using the chosen range of temperatures in Athena. Smaller variations were then applied to the curve which fit best with the actual R_s values, in order to achieve further optimization. Similar fitting procedures have been performed in previous publications [20].

4.1.2 Details of Athena simulations

Two different values were chosen for the diffusion time, 25 and 37.5 minutes, both for which a range of five temperatures was chosen; from 790 to 910 °C, with steps of 30 °C. This range of temperatures and diffusion times coincides with the experimental laboratory work and hence enables comparison between the two sets of results. Because the default properties of the simulated oxide layer differed from the P509 phosphorus solution and thereby had to be altered, a thorough effort was made to obtain a good approximation that would fit results from the full range of 10 different chosen in-diffusion parameter sets.

As described in section 2.3, the diffusivity increases with temperature. Therefore, the expected result of the experiments is a larger extent of dopant in-diffusion for a higher temperature and a longer diffusion time.

Parameters stated in the simulations were

- Background doping of bulk silicon
- Concentration of phosphorus in oxide and thickness of the oxide layer
- Ambient gases
- Diffusion temperature and time
- The diffusivity coefficients D^0 and E_A

4.2 Simulation of substrate lifetime

In the basic lifetime theory given in section 2.2, it was stated that the front-surface field reduces surface recombination by moving carriers away from the surface, where the recombination is large. A high effective lifetime is a critical requirement in back-contact solar cells because of the necessary through-wafer carrier transport. However, the presence of dopants in the substrate contributes to a reduction of the effective lifetime. Donor dopants establish energy states close to the conduction band, and acceptor dopants establish states near the valence band. The optimal effective lifetime is therefore a result of the balance between surface recombination and recombination caused by dopants. This section describes the simulation software used to find effective lifetimes based on the dopant profiles.

4.2.1 Lifetime simulation in PC1D

The program PC1D enables simulation of one-dimensional semiconductor structures [21]. PC1D is a popular tool for investigating concepts within photovoltaics, commonly used for interpreting experimental data [22]. Although the geometric configuration of the solar cell is limited to specifying its thickness, PC1D is still a powerful software due to the ability of treating a range of parameters, regarding the material properties, dopants, and manners of charge carrier excitation.

In the present work, a structure consisting of one in-diffused junction on each side of an n-type wafer was to be simulated. The layout of the structure when simulated in PC1D is shown in fig. 4.2. The software involves simulation of a light flash with adjustable properties. Data for the photoconductance and electron-hole-pair generation are extracted from the simulation. The effective lifetime is then found using processing tools which are based on the Sinton WCT-100 software (section 3.3.3).

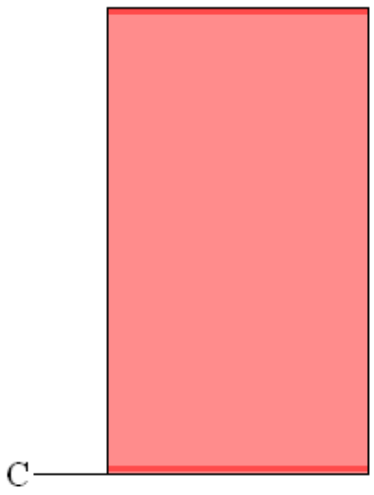

Figure 4.2: The one-dimensional layout represented in PC1D. The figure shows a n^+-n-n^+ structure. A darker red color represents heavier donor doping.

4.2.2 Details of PC1D simulations

The value of surface recombination velocity needed to be set for each PC1D simulation. A high SRV value corresponds to a poorly passivated surface, i.e. a large dependence of the effective lifetime on the surface properties, while a low SRV value implies good passivation. In previous PC1D simulation studies of back-junction cells performed by Nichiporuk *et al.* [23], surface recombination velocities of 100 cm/s were used for the front and back surfaces. This value was used as the minimum SRV value in the present work, due to an assumed significant level of surface contamination from the conditions in the laboratory as described in section 3.4.2.

It was desirable to obtain an answer to whether and to which extent an in-diffused front surface field is advantageous. This would in turn argue for the case of front surface in-diffusion to support the theoretical foundation and previous reports on this issue, considered in section 2.6.2. Data from PC1D simulations were therefore used to plot the relationship between surface recombonation velocity and the effective lifetime.

Table 4.1 shows the parameters which were used for the simulations. The wafer thickness, stated approximately by the wafer manufacturer, was confirmed by a thickness measuring probe. The bulk resistivity of $\rho = 2$ Ω-cm yields a background doping of $n_0 = 2.4{\times}10^{15}$ cm^{-3} when the relationship between these quantities, given by $\rho = (q\mu_n n_0)^{-1}$, is applied [7].

As mentioned in the Theory chapter (2.5.2), SunPower Corp. produces and

Parameter	*Value*
Wafer thickness	300 μm
Bulk resistivity	2 Ω-cm
Bulk lifetime	700 μs
SRV	100, 500, 1000 cm/s

Table 4.1: Details of the PC1D simulations.

markets high-efficiency BJ solar cells. The bulk lifetime of the starting wafer material used in this manufacture exceeds 1 ms [24]. Prior to in-diffusion, some passivated wafers were characterized through WCT-100 measurements. The results showed that the lifetimes were relatively low; values averaging to approximately 650 μs were found on well-passivated samples. Based on these findings and including a lifetime margin due to surface recombination, the bulk lifetime in simulations was set to 700 μs.

The photoconductance σ_L and the photogeneration current J_{ph} were extracted from each simulation when the given input parameters were applied. This allowed for lifetime calculations utilizing the qssPC method. A separate calculation for processing of these data, based on the calculation software for the WCT-100 apparatus, was utilized. Each value of light intensity yields a certain excess carrier density for a given bulk lifetime and surface recombination velocity. From eqs. 3.1 and 3.2, the effective lifetime may hence be found with respect to Δn.

In the τ_{eff} vs. Δn plots, an excess carrier density of $1{\times}10^{14}$ cm^{-3} was chosen. This is a likely value when unconcentrated sunlight is assumed.

Chapter 5

Results and discussion

Results are presented in this chapter and subsequent discussions are given on each issue. The results from measurements of sheet resistance and effective lifetime are first considered. Some aspects regarding the phosphorus spraying process are then discussed, followed by a treatment of the dopant profile simulations. Finally, the discussion on the effective lifetime is given which comprises two main analyses; a comparison of the two lifetime computation methods due to the observation of unreliable initial lifetime results, and the investigation of dopant profile with respect to lifetime.

5.1 Characterization

A detailed description of the investigation of sheet resistance and effective lifetime, for p-type and n-type wafers respectively, is given in section 3.3. The results from measurements are presented and discussed in this section.

5.1.1 Sheet resistance mapping

Fig. 5.1 shows a mapping image from the Semilab SHR. The spatial variation in sheet resistance on a square, 60-mm p-type wafer sample can be seen represented by a color chart. The histogram on the right in the figure is a useful representation of the homogeneity of sheet resistance values in the map.

In order to achieve correct Semilab measurements it was necessary to calibrate the apparatus. During calibration, the sheet resistance is measured at a certain point on the wafer. The position of this point is not accurately

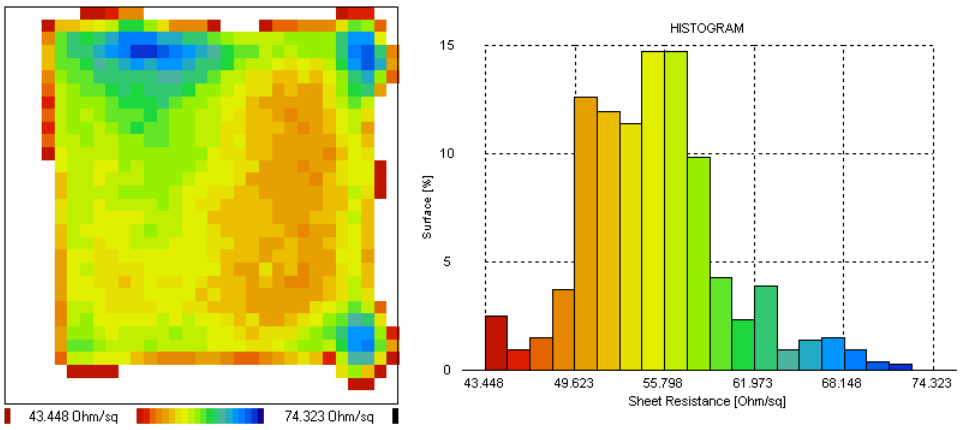

Figure 5.1: Map of the sheet resistance in a wafer with an average R_s value of 55 $\Omega/\square$ and the resulting histogram.

known. This is because of the manner of characterization used in Semilab measurements, briefly described in section 3.3.2, which outputs a sheet resistance based on the resultant voltage potential of a certain circular area on the wafer. During conduction of the calibration procedure it was discovered that spatial variations of the sheet resistance on wafers used for calibration were too large. Consequently, the Semilab measurements gave inconsistent results. To ensure a good accuracy, measurements using Semilab were therefore limited to considerations of the homogeneity, and four-point probing was chosen as the main tool for obtaining the values of sheet resistance. Cases with large variations on the surface were however easily discovered using Semilab, regardless of the erroneous calibration; this way, the Semilab measurements was a helpful tool in the measuring process.

5.1.2 Sheet resistance measurements

Four-point probe measurements were conducted on wafer batches of which sufficient homogeneities could be ensured by use of the Semilab characterization. For sample batches with too high spatial sheet resistivity variations, the wafers were discarded and new samples were processed. Sheet resistance data versus diffusion temperature for diffusion durations of 25 minutes and 37.5 minutes are shown in Fig. 5.2.

As can be expected from Eq. 2.4 when recalling that R_s is directly related to the amount of in-diffused dopants, the sheet resistance decreases exponentially with increasing temperature. Also, the resulting in-diffusion increases with diffusion time, suggesting a good reliability of the measurements.

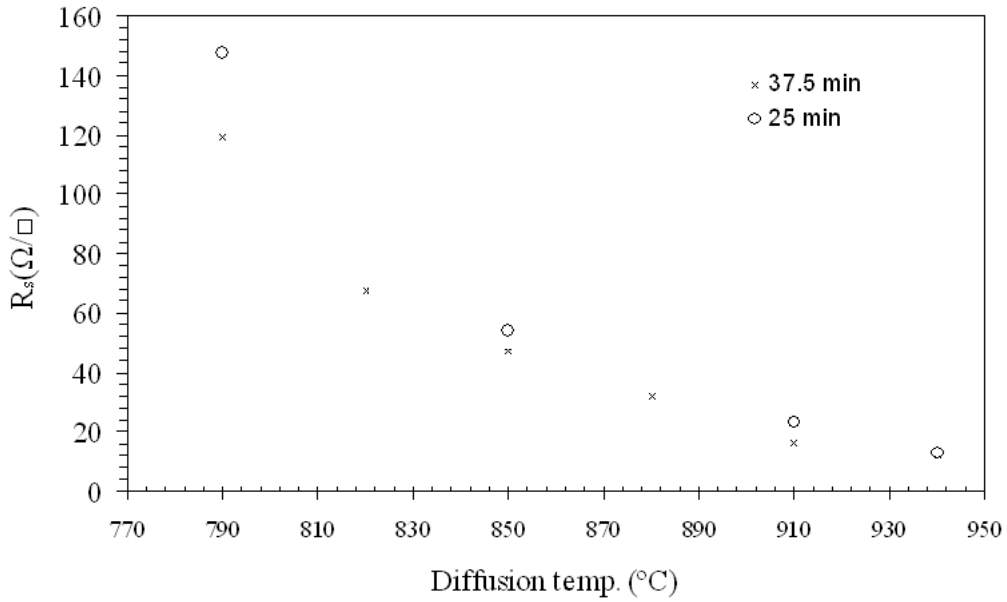

Figure 5.2: Figure showing sheet resistance vs. diffusion temperature as measured with 4-point probe, for the two chosen diffusion times.

5.1.3 Investigation of phosphorus glass

The front surface of two p-type samples were investigated by the use of a scanning electron microscope (SEM) after the deposition and baking of phosphorus sol. Resulting images are shown in Fig. 5.3. The silicon material, in the lower part of the figures, can be distinguished from the glass layer above. It can be seen in the left figure, 5.3(a), that the thickness of the oxide layer is inhomogeneous. It is also clear from the image that there are variations in the glass layer, suggesting that it exhibits a certain porosity. Figure 5.3(b) indicates that the oxide layer thickness is dependent on the wafer surface topography; the layer is thicker over depressions in the underlying Si material and thinner over elevations. This suggests that a flat surface is an important factor for the homogeneity of the glass layer.

The inhomogeneity of glass is in agreement with the inhomogeneous sheet resistance of the in-diffused region. It must be noted that the lateral dimensions covered in the SEM images are lower than the length scales that can be measured by the Semilab SHR; however, we may assume that macroscopic inhomogeneities are present as well based on these images. This gives reason to argue that the unsatisfactory level of sheet resistance homogeneity is caused by the spraying process. The SEM images are also helpful in the determination of a range for the possible thickness of the oxide layer for Athena simulations. Consideration of Figs. 5.3 and additional SEM images,

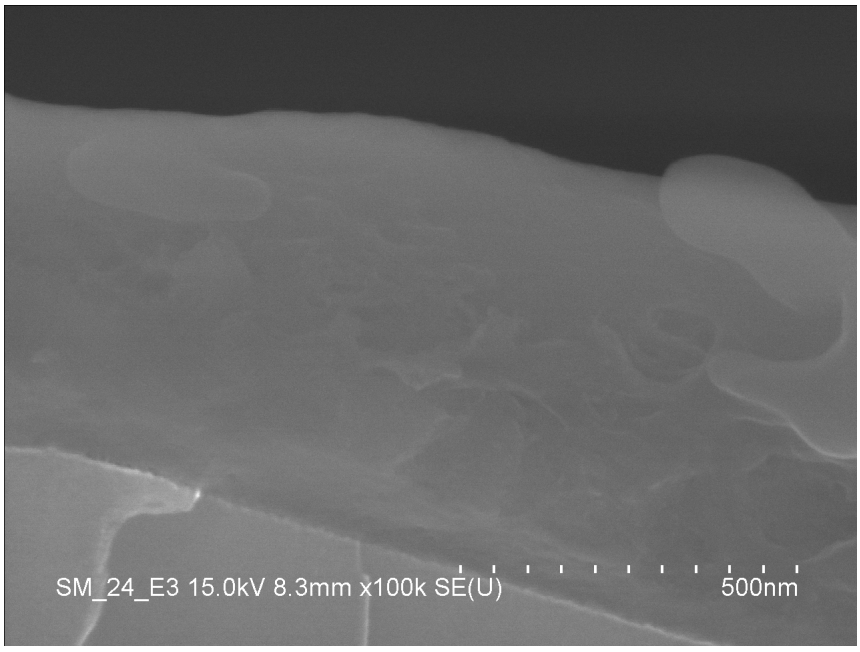

(a) Close-up image of the phosphorus glass.

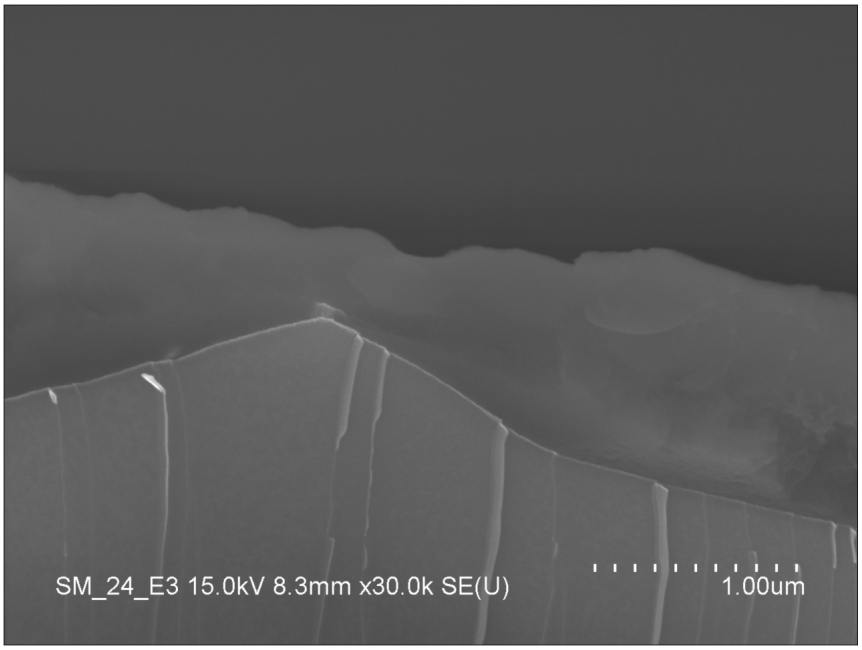

(b) An elevation in the Si wafer surface, resulting in a thin glass layer.

Figure 5.3: SEM images.

displayed in the Appendix, indicates a thickness between 0.3 μm and 1.5 μm.

5.1.4 Measurements of effective lifetime

The Sinton WCT-100 apparatus was used to measure effective lifetimes after passivation and tempering of n^+-diffused n-type samples. The chosen duration of diffusion for these experiments was 25 minutes. The results of the measurements are shown in Fig. 5.4.

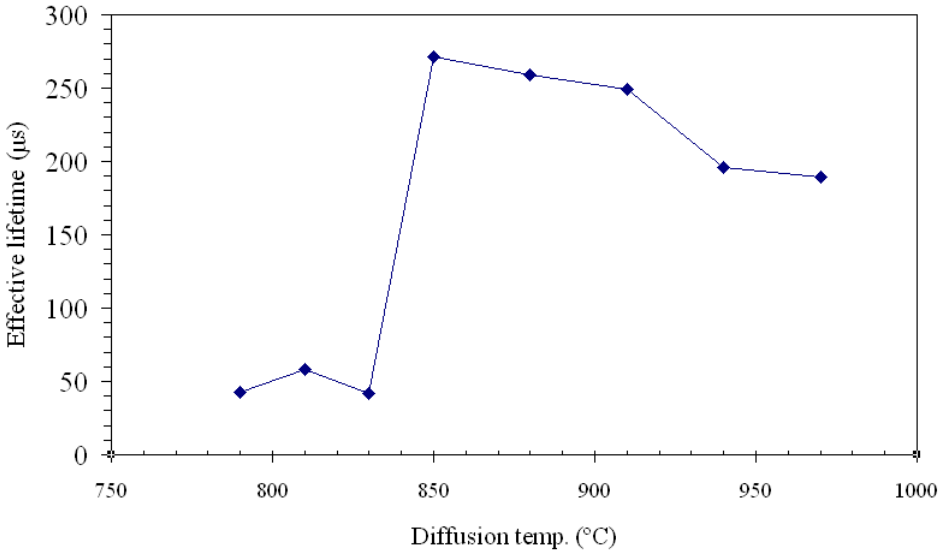

Figure 5.4: The measured lifetimes after in-diffusion of phosphorus in n-type samples with respect to diffusion temperature.

The bulk lifetime is assumed to be approximately 650 μs, as mentioned in sec. 4.2.2. The maximal lifetime seen in Fig. 5.4 is 271 μs, which was measured for a diffusion temperature of 850 °C. Thus, from these results, dopant in-diffusion clearly yields high carrier recombination. The assumed bulk lifetime was also measured at the IFE laboratory, but without subjecting the wafers to large temperatures prior to measurements. The in-diffusion of unwanted impurities due to contamination in the laboratory thus may be assumed as a contribution to the reduction in lifetime. This issue is treated more closely later in this chapter.

Also seen in the figure are significantly lower effective lifetimes for the range 790 °C-830 °C than for higher temperatures. This indicates that the measurements are more prone to error for these temperatures because of the low depth of the in-diffused dopant profile. A possible explanation lies in the low levels of diffusion which occur at low temperatures. Considering

the slight inhomogeneous dopant spraying pattern from the Sprutus apparatus, it is reasonable to assume that there are small areas on the wafer surface in which no phosphorus is in-diffused; thus, the relative change in dopant concentration in the plane of the surface may be very large. Fig. 5.5 shows, schematically, a hypothetical situation where phosphorus has been in-diffused into the wafer exclusively at a certain spot. Arrows indicate the resulting electric field, which acts on charge carriers. Because of the dopant gradient in the plane of the surface, it is probable that the doped area causes charge carriers to move within this plane rather than downwards in the wafer, in which case the effective lifetime is reduced due to surface recombination.

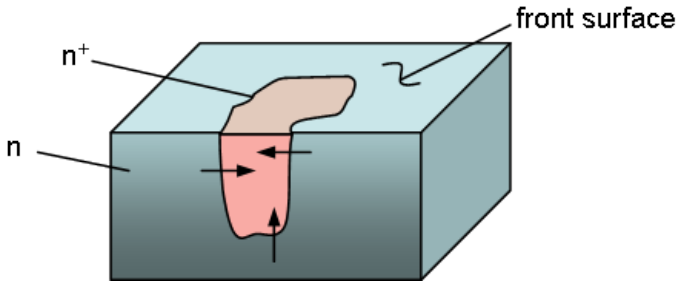

Figure 5.5: Schematical representation of a wafer segment in which a spot of phosphorus has been in-diffused. There is reason to assume that such an in-diffusion will occur at low temperatures. The electric field flowing from lightly to heavily n-doped areas is indicated by arrows.

The immediate conclusion from the lifetime measurement is that an optimal diffusion temperature, with the provided diffusant and duration of diffusion, seems to be lower than 850 °C . We have observed in Fig. 5.2 that the sheet resistance for a 850 °C in-diffusion is only 44.8 Ω/□. From this, it is clear that the experimental lifetime measurement results do not provide good information about the relevant range of temperatures. However, for higher temperatures the lifetime decreases with temperature, which is as expected: An increasing extent of dopant energy levels within the band gap causes increasing recombination. We can expect a higher lifetime if a better spray-on homogeneity is achieved.

5.2 Phosphorus spray-on source

Optimizing the parameters of the Sprutus apparatus from the default values (see section 3.4.2) resulted in the findings listed below.

- Setting the number of spraying repetitions to four showed that cracks formed in the glass layer after baking at this layer thickness. When

using two spraying repetitions, no cracks were visible while the wafer surface still appeared to have a full coverage of glass.

- The air spray pressure visibly yielded a better performance when it was decreased from the default values. When utilizing the pressure value which was set from previously conducted optimization attempts, the P509 spray was clearly inhomogeneously sprayed. After reducing the pressure, an increased homogeneity resulted. The reason for this can be seen by considering the sheet resistance maps; Fig. 5.6 displays the Semilab SHR map from a test sample. Sheet resistance values are higher at the wafer center, along the path of spraying. This suggests a somewhat higher air flow directly underneath the nozzle than in other directions, causing more liquid to be directed towards the wafer sides.

- When the concentration of P509 solution in proportion to ethanol was increased, the performance of the spraying process was changed. Spray was more unevenly distributed and clogging of the nozzle occured rapidly. It was concluded that the dilution ratio between phosphorus and ethanol of 1:4 was a well optimized concentration, yielding a low degree of clogging.

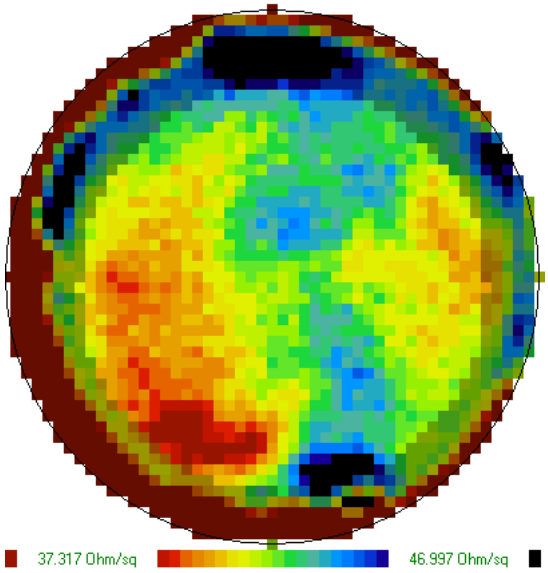

Figure 5.6: Map of the sheet resistance in a circular test wafer. Sheet resistance values are higher along the path of spraying, which suggests that the air spray pattern is uneven.

Optimization of the parameters was a difficult issue, due to mutual dependence of certain parameters; also, the relation between chosen values and

physical performance was often nonlinear. Moreover, clogging of the spray nozzle introduced small, but significant, changes in performance over time.

5.3 Athena simulations

In this section, the simulation of dopant profiles is considered. A discussion is carried out regarding the simulation of the P509 sol as a phosphorus-doped oxide layer. Subsequently, the dopant profiles resulting from the fitting procedure based on sheet resistance measurements are treated.

5.3.1 Spray-on phosphorus modelled as SiO_2

As described in section 4.1.1, the P509 sol exhibits an increase in viscosity during baking. The diffusion properties of the resulting solid, represented by the prefactor D^0 and the activation energy E_A, are expected to be somewhat similar to the properties of SiO_2, but may differ to an extent which is difficult to calculate explicitly. This is described in section 4.1.1. The P509 is a complex composition; thus, assessing the motion of phosphorus atoms in the sol is difficult. The diffusivity was therefore found empirically by means of a fitting procedure using Athena simulations. Because monocrystalline silicon was used, the occurence of irregularities like grain boundaries and defects is small, which makes it reasonable to assume that the experimentally obtained dopant profiles equal the profiles found in simulations.

Parameters for material properties and ambient gases were set to fixed values for the full range of different temperatures, as shown in table 5.1. Fitting simulations with the measurements made from laboratory samples proved to be a rather complex process, as it was necessary to perform multiple simulations with varying parameters. The Athena script for a simulation of phosphorus in-diffusion is given in the Appendix.

With no altering of the diffusivity coefficients from the default oxide values, the simulated sheet resistance ended up too large for all temperature values. The oxide thickness utilized was then 1 μm, based on the assumed average thickness from SEM images. Using a larger value for the diffusivity (i.e. either increasing D^0 or decreasing E_A) was then attempted. However, the resulting range of sheet resistance did only coincide for one value of temperature, which meant that a mutual weighing between D^0 and E_A was necessary. Some different combinations of the two diffusivity parameters, all yielding the same diffusivity at a certain temperature, were then utilized in simulations to assess this discrepancy. The parameter set shown in table 5.1 resulted after mutually adjusting not only D^0 and E_A, but also several

Parameter	Value
Bulk background doping (boron)	3.5×10^{15} cm^{-3}
Dopant conc. in oxide	4.0×10^{20} cm^{-3}
Thickness of doped oxide	0.5 μm
Ambient gases (percentage):	
Nitrogen	78.5 %
Oxygen	21 %
Water vapour	0.5 %
Prefactor D^0	0.5 cm^{2}s^{-1}
Activation energy E_A	3.1 eV

Table 5.1: Simulation results for the front surface sheet resistance for some given values of diffusion temperature and time.

attempts of varying the oxide thickness and the doping of the oxide layer within a realistic range (see section 4.1.1).

5.3.2 Final dopant profiles

Fig. 5.7 shows the previously displayed sheet resistance data, accompanied by the resistance results from Athena simulations after fitting of the diffusivity parameters.

The resulting dopant profiles after the fitting process are presented in Fig. 5.8. The concentration shown is the *active* phosphorus atoms, i.e. the dopants that are part of the lattice and hence contribute with charge carriers to the dopant energy level. As expected, the extent of in-diffusion is larger for higher temperatures. Note that the peak concentration remains within a relatively short range, 2-3.5$\times10^{20}$ cm^{-3}; that is, the junction depth is altered with respect to diffusion temperature, while the peak concentration is kept approximately constant.

For a consideration of the altering of in-diffusion properties, Fig. 5.9 shows the resulting dopant profile when the default diffusivity parameters for silicon dioxide are utilized. Clearly, the amount of in-diffused phosphorus is then lower; thus, the diffusivity in P509 is larger than in silicon dioxide. To explain this, a consideration of the motion of phosphorus atoms in the glass layer is necessary. Due to the increasing viscosity in the sol-gel with respect to the duration of baking, it is probable that diffusion of phosphorus molecules occurs at a faster rate in the beginning of the diffusion process, although slowing down as heat is continuously applied.

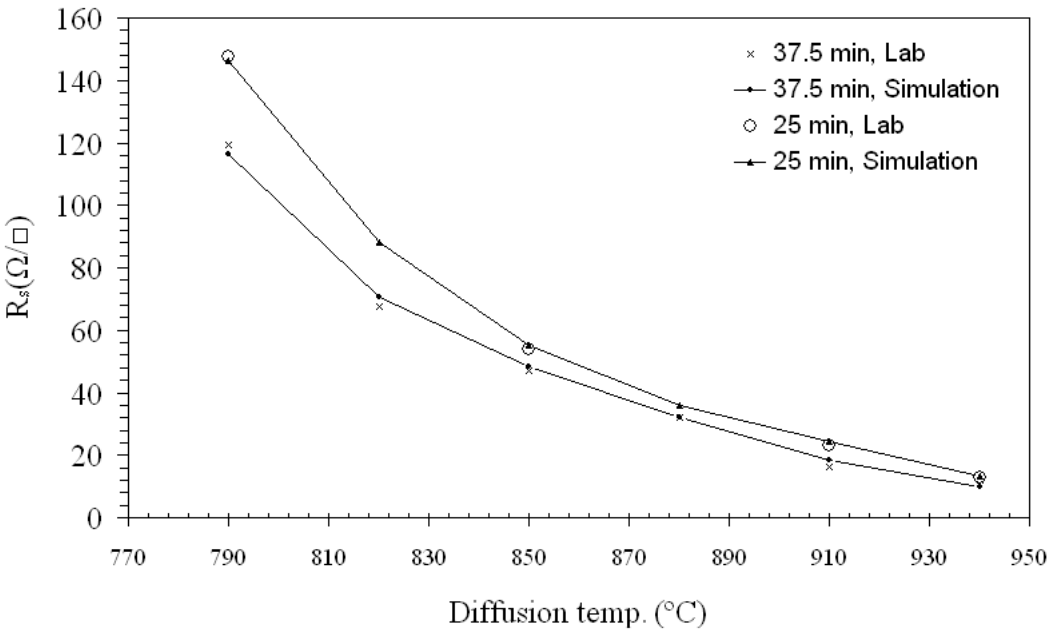

Figure 5.7: Figure showing sheet resistance vs. diffusion temperature as measured with 4-point probe (dotted) and the simulation results after adjustment to fit experimental results for both diffusion times (lines).

5.4 PC1D simulations

In the first phase of the PC1D simulations, an examination was carried out concerning how the choice of lifetime calculation method affects the reliability of the results. As described in section 2.3.3, approximation of the dopant profile may be done based on the complementary error function (erfc). The effective lifetime was simulated with respect to the sheet resistance using built-in erfc profiles in the software, in order to investigate and compare some general cases and to obtain a reference for the further work. The simulation results are treated in this section. Finally, the results of lifetime analysis made from dopant profiles from Athena simulations are presented and discussed.

5.4.1 Discussion on lifetime computation methods

Two methods for obtaining the effective lifetime of a silicon wafer are described in section 3.3.3. The photoconductance decay method gives the lifetime as a result of the decay slope of photoconductance transients when excitation is generated from a flash lamp. The quasi-steady-state photoconductance method assumes approximate steady-state conditions and makes

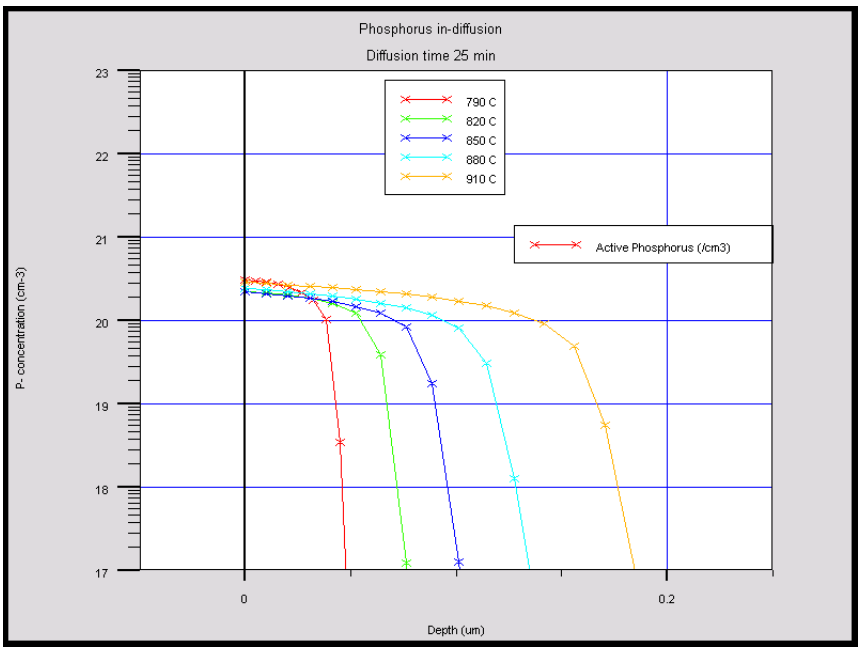

(a) 25 minutes

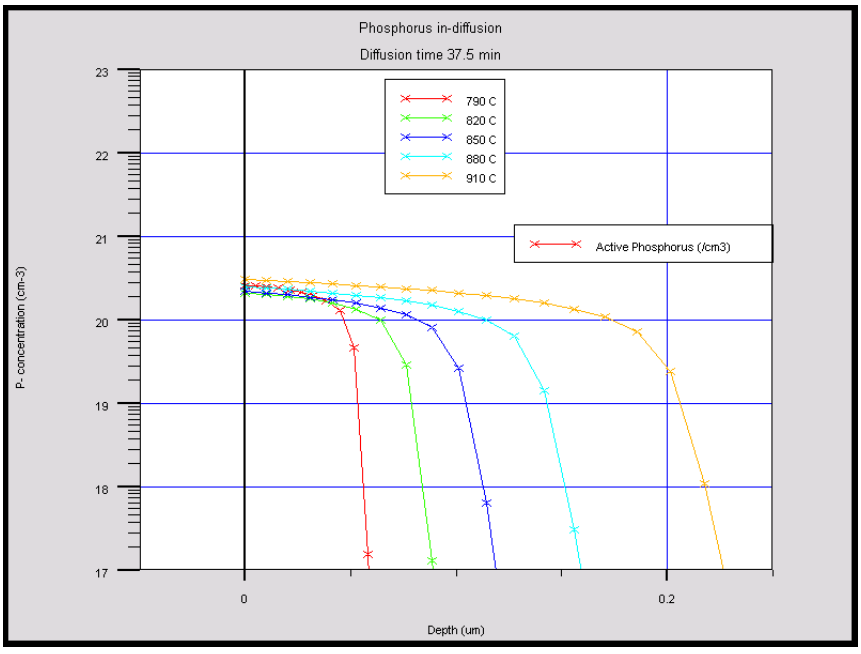

(b) 37.5 minutes

Figure 5.8: Athena plots showing dopant profiles inwards from the silicon surface, i.e. the dopant concentration with respect to wafer depth, at the two durations of diffusion.

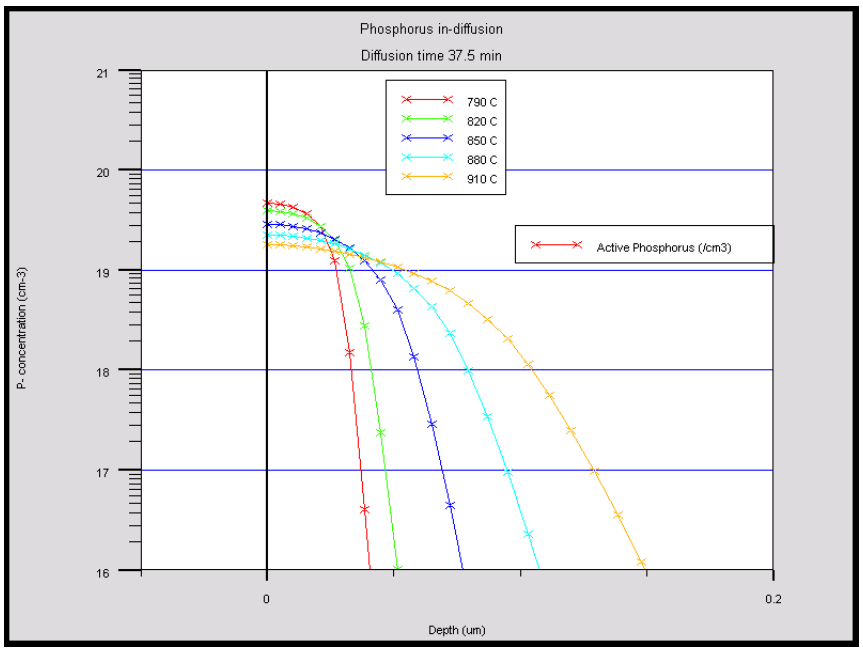

Figure 5.9: Athena plot of the dopant profile where diffusion parameters for SiO_2 are used.

use of generation-recombination balance equations to find the lifetime. In the processing of data from PC1D simulations, qssPC was the method initially utilized; however, as shown subsequently, the photoconductance decay method was found more appropriate and was finally the chosen means of calculation. As in the case of experiments, using one of these two methods in PC1D means that the simulated illumination must be in the form of a flash. The program enables for assigning the temporal properties of the flash, i.e. the light intensity versus time.

Testing the lifetime calculation software initially proved that the simulated lifetime values were too high to be correct. As carriers are assumed to be close to steady-state, the qssPC method does not apply to fast decaying light pulses. Longer decay lengths were therefore tested; this would optimally give quasi-steady-state conditions. The result is shown in Figs. 5.10 (a) and (b). Excess carrier densities of $1{\times}10^{14}$ cm^{-3} are assumed in interpretations of lifetime simulations (see sec. 4.2.2).

Fig. 5.10(a) shows that the effective lifetime exceeds the bulk lifetime, which is clearly incorrect according to Eq. 2.3. When the flash decay is prolonged to twice the original length, a lifetime decrease follows as seen in Fig. 5.10(b). However, prolonging the decay lengths further did not give useful results. The number of possible data points in PC1D is limited, so that no data was

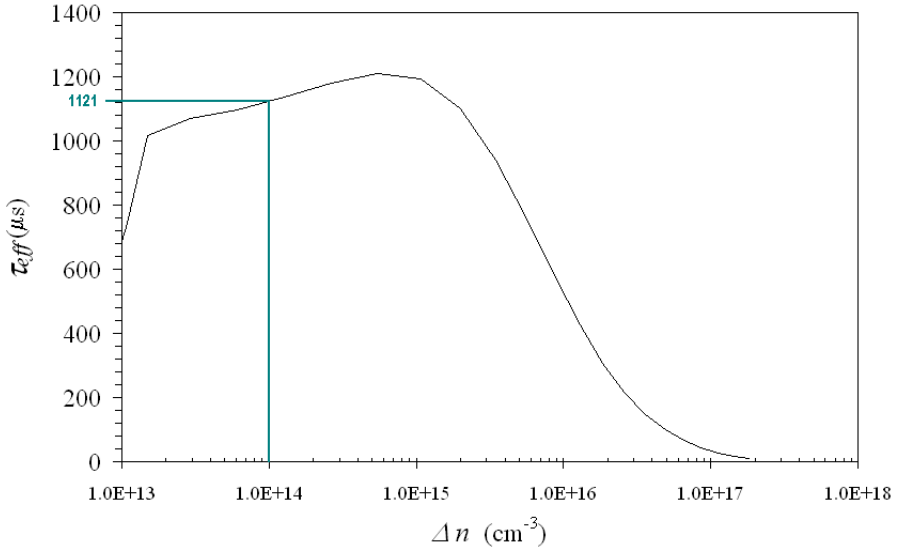

(a) Original flash decay

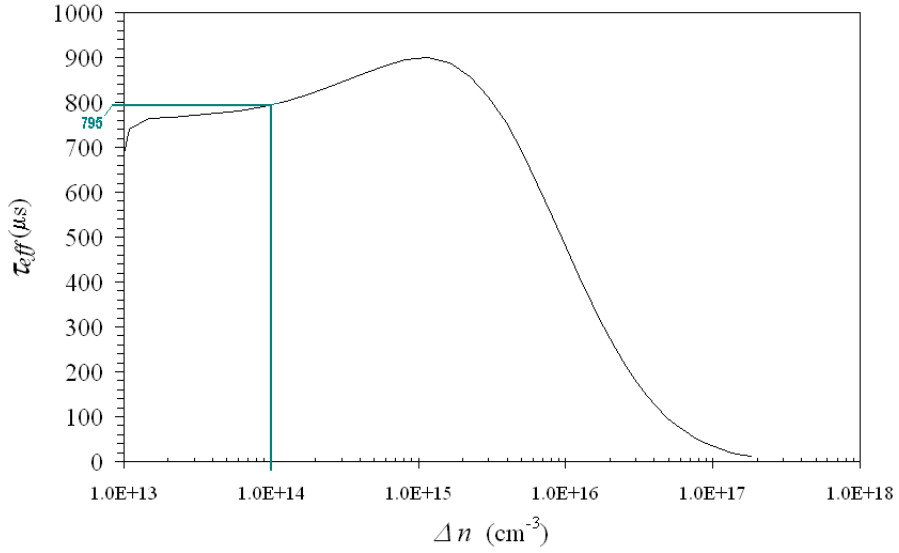

(b) Flash decay length doubled

Figure 5.10: Lifetime simulations with respect to injection level using different flash decay lengths.

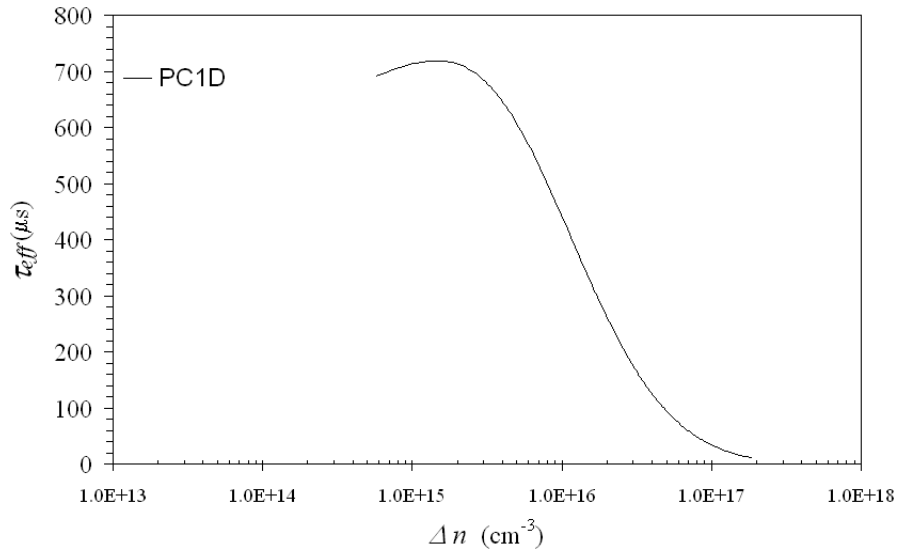

Figure 5.11: Lifetime simulation with respect to injection level using a long flash decay length. The number of allowed data points in PC1D is too low for this case; concequently, no lifetime data is obtained for $\Delta n = 1 \times 10^{14}$ cm^{-3}.

attained for the lower injection levels which apply at lower light intensities. See Fig. 5.11.

In order to obtain lifetime calculations that yielded results for all injection levels, the photoconductance decay method was used instead. The lifetime then assumed lower values. Figs. 5.12 and 5.13 allow for a comparison of the two cases. The former figure shows that the qssPC method yields lifetimes exceeding the bulk lifetime, while the latter figure shows the lifetimes calculated with the photoconductance decay method which gives lifetime values below the bulk lifetime. However, Fig. 5.12 is illustrative for the general dependence of lifetime on the SRV value. Obviously, a lower surface recombination velocity S_0 yields a higher lifetime. In addition, the figure shows that for a higher surface recombination velocity, the optimal lifetime occurs at a higher level of in-diffusion. The initial, short pulse decay length was utilized in these simulations, since no quasi-steady-state requirement applies. For the remainder of the results, the photoconductance decay method has been used.

Two different values for the surface recombination velocity S_0 are used in Figs. 5.12 and 5.13. As described in section 4.2.2, it is assumed that the passivation yields a SRV value higher than 100 cm/s, based on existing litterature on simulations of back-junction cells.

In Fig. 5.13, the effective lifetime dependence on the sheet resistance is also implemented (upper axis). For lower SRV values, the lifetime is high for

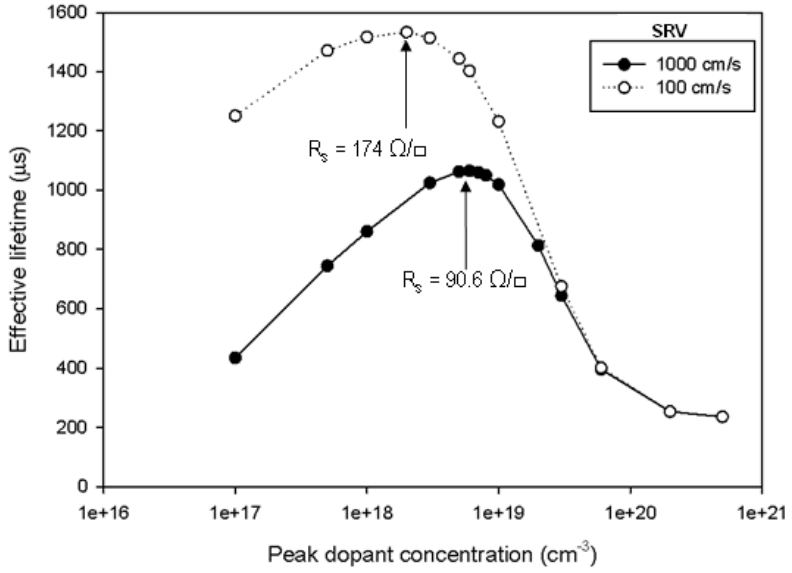

Figure 5.12: PC1D simulation results showing the lifetime dependence on the dopant concentration with the quasi-steady-state photoconductance method.

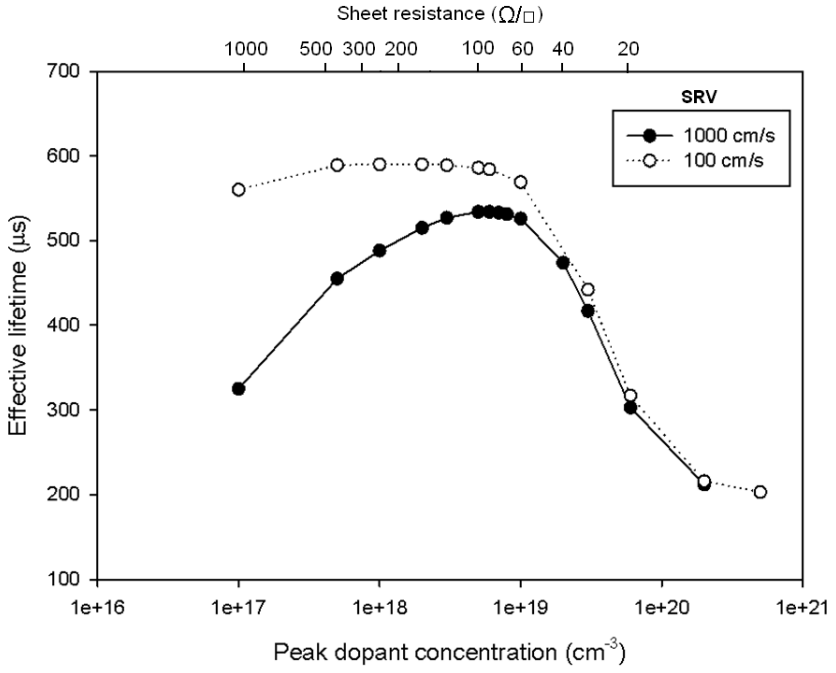

Figure 5.13: PC1D lifetime simulation results with the photoconductance decay method.

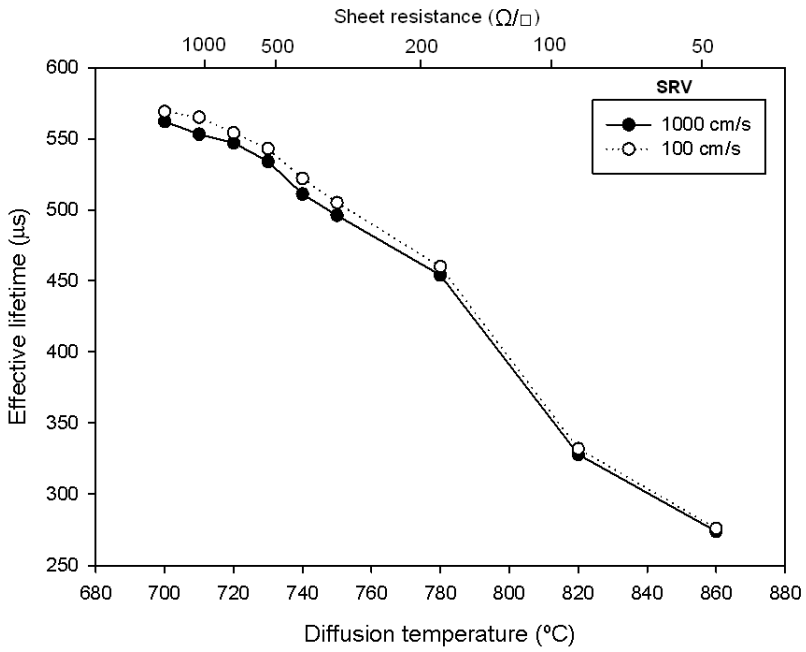

Figure 5.14: PC1D lifetime simulation results based on dopant profiles from Athena, i.e. with the parameters given in Table 5.1.

large sheet resistances. This is as expected; a low degree of recombination leads to a low impact from the front surface field.

The maximal lifetime is found for the sheet resistance range 90-100 Ω/□ in the case $S_0 = 1000$ cm/s. For the case of a low SRV, the range of maximal sheet resistances is larger, 100-400 Ω/□. This implies that a relatively high sheet resistance is necessary for good FSF passivation. Findings have recently been published within BJ solar cell research which report of optimal sheet resistance values of 148 Ω/□ [25].

The dopant profiles which were found in Athena simulations (Fig. 5.8) were loaded into PC1D. The simulations allow for effectively prolonging the range of temperatures; data points were collected for temperatures ranging from 700 °C to 860 °C. Effective lifetimes were then calculated, shown in Fig. 5.14. Comparing these results with the measured lifetimes from the WCT-100 apparatus in Fig. 5.4 shows a good agreement; at a diffusion temperature of 850 °C, the measured and simulated lifetimes are 271 μs and 280 μs, respectively. Assuming that the simulation is correct based on this observation, we may conclude that the lifetime is heavily impacted by dopant energy levels at 850 °C.

In order to obtain the relationship between sheet resistances and diffusion

Depth factor (μm)	R_s ($\Omega/\square$)	$\tau_{\text{eff,front}}$ (μs)	$\tau_{\text{eff,back}}$ (μs)
0.001	66,120	91	68
1.0	66.1	85	67
3.0	22.0	85	67
10	6.6	64	67

Table 5.2: Simulations of the effective lifetime for some sheet resistance values, where only the front or only the back surface of the wafer is phosphorus diffused. 'Front' and 'back' refer to the wafer side for which the in-diffusion is done. Illumination is incident on the front side.

temperatures, it was necessary to prolong the plot of sheet resistance so that lower temperatures were included. This is shown in the Appendix.

5.4.2 Discussion on simulation of the front-surface field

Utilization of built-in erfc profiles allows for a reliable investigation of the general impact of a surface field. Table 5.2 shows a comparison of the lifetimes, given in μs, when a dopant region is present exclusively at one side of the Si wafer. The dopant diffusions used are all erfc profiles, with a peak concentration of $1{\times}10^{19}$ cm^{-3}. For low values of the dopant depth, it is readily seen that the front surface diffusion gives a higher yield in terms of effective lifetime than diffusion on the backside. This is as expected, due to the large extent of photogeneration at the front compared to the back side. The diffused dopant region at the back surface does not give large variations in lifetime with respect to dopant depth, and exceeds the only-front-diffused case for larger dopant depths. However, as has been shown above, the front surface sheet resistance should be large for an efficient front-surface field at moderate surface recombination velocities. Lifetimes following from front diffusion are larger than for back diffusion for the relevant range of sheet resistances.

In Fig. 5.15, the effective lifetime with respect to the junction depth is shown for a peak dopant concentration of $4{\times}10^{20}$ cm^{-3}, based on the concentration assumed in experiments. The line between the first two data points, at which the junction depth is increased from 0 to 1 nm, clearly does not fit into the trend of the plot. To assess this discontinuity, the treatment of dopant profiles in PC1D must be considered. A low junction depth value, i.e. a narrow depth, leads to a very abrupt junction when the erfc profile is utilized. The junction abruptness decreases when the depth is increased. Since the peak dopant concentration is equal in all cases, a larger abruptness contributes to increasing the surface field. This contribution is countered by the total amount of doping, which obviously is larger for a larger junction

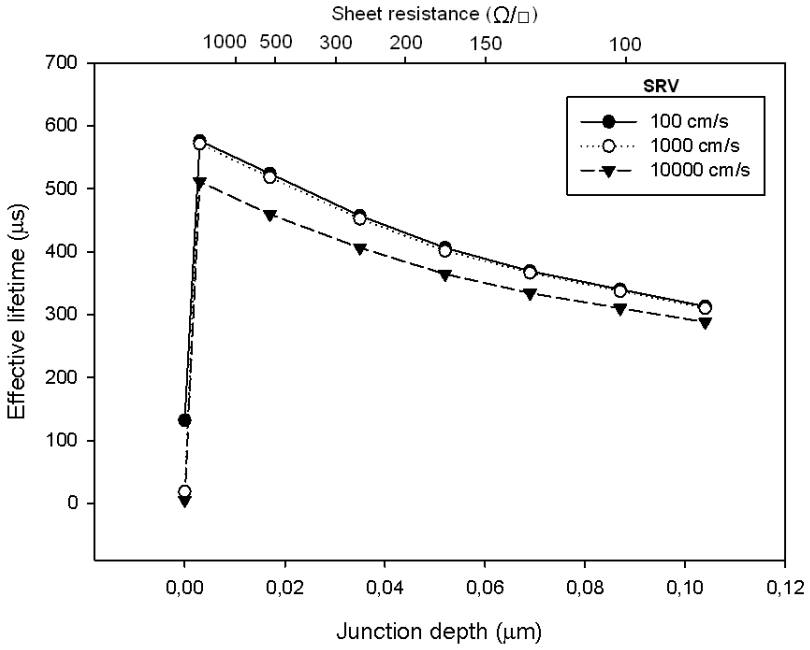

Figure 5.15: Lifetime simulation results based on erfc dopant profiles, where the peak dopant concentration is kept constant at 4×10^{20} cm^{-3} and the junction depth is varied. Three different surface recombination velocities have been used.

depth. However, the observation that there is no continuous increase in lifetime with respect to junction depth indicates that the latter contribution has a low impact. It should also be noted that at a junction depth of zero, i.e. when no diffusion is present at either side of the wafer, the lifetime is very low for SRV values in the order of 1,000 cm/s. Thus, most of the photoexcited charge carriers recombine in vicinity of the front surface.

It was desirable to focus on the applicability to the practical case. Therefore, only realistic sheet resistance values are represented in the PC1D simulations: The resistance is limited to a range from 10 to 1000 Ω/□. The ranges of the parameters (e.g. junction depth in Figs. 5.15 and 5.16) are consequently quite different for each case of peak dopant concentration.

In Fig. 5.16, the lifetime is investigated for cases of high surface recombination velocities. A lower peak concentration (1×10^{19} cm^{-3}) is used. In order to obtain relevant sheet resistances, the junction depths represented are unequal in the two figures, as mentioned above; that is, using lower dopant concentrations requires a deeper diffusion. This way, the junction abruptness is decreased. Note that only nonzero depths are plotted in this graph; with the undiffused case included as well, a similar discontinuity in lifetime as seen in the previous plot would be expected. The three surface

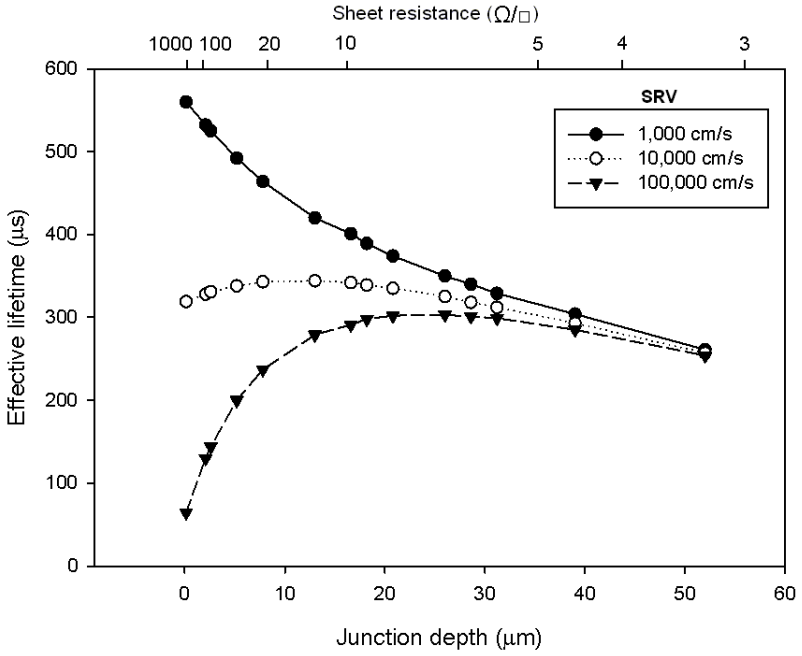

Figure 5.16: Lifetime simulation results for cases of high surface recombination velocities, where the peak dopant concentration is kept constant at 1×10^{19} cm^{-3} and the junction depth is varied.

recombination velocities utilized yield largely dissimilar results of the lifetime versus the junction depth, which in combination are very illustrative for the dependence of lifetime on S_0:

- For S_0 =1,000 cm/s, the lifetime is continuously decreasing with respect to junction depth. The surface recombination is clearly not high enough for the lifetime to exhibit a maximal point.
- Increasing the surface recombination velocity 10 times yields a maximum lifetime value for a sheet resistance of 13.2 Ω/□. The lifetime remains relatively stable for decreasing junction depths from this maximal point, which implies that the decrease in lifetime caused by surface recombination balances the effect of the front surface field.
- A surface recombination velocity in the order 1×10^5 cm/s yields a maximal point in lifetime at a lower sheet resistance; 6.6 Ω/□. Hence, the surface recombination has a large impact and a very deep diffusion is necessary for the dopant atoms to cause more lifetime reduction than the surface recombination.

Generally, the optimal sheet resistances observed above are lower than what

was seen in Fig. 5.13. This is due to the high SRV values. The case of $S_0 = 1 \times 10^5$ cm/s corresponds to a very poor passivation or an unpassivated surface. Hence, in such cases, Fig. 5.16 gives a good indication of which junction depth to choose for the front surface field. However, using a range of diffusion depths is seemingly not a good means of front surface field optimization when we assume a good surface passivation and that the conditions for sol deposition at the IFE laboratory apply. Ideally, the dopant sol deposition should be homogeneous over the area of the wafer - assuming that this is the case, the results obtained in this study show that the sol layer should be as thin as possible.

5.4.3 Optimization of effective lifetime

The results from simulations where the junction depth is varied clearly differ from simulations where the peak concentration is varied. Altering the peak concentration leads to a certain sheet resistance, or a range of sheet resistance values, for which the effective lifetime is optimized. Particularly for the case of a high surface recombination velocity, optimization based on the peak concentration is effective. Altering the junction depth, on the other hand, yields no maximal point in lifetime with respect to sheet resistance except in the case of very high surface recombination velocities, i.e. for unpassivated or poorly passivated surfaces. This situation was clearly observed in Fig. 5.14, where the Athena simulations were made based on alteration of the junction depth.

This shows that the choice of parameter for altering the sheet resistance is very important for the optimization of lifetime. Considering the observation described above with regard to the results from experimental work, we recall from Figs. 5.8 that these dopant profiles, which are assumed to be resulting from the physical in-diffusion of phosphorus, all exhibit approximately equal peak dopant concentrations. A range of diffusion temperatures thus yields a range of junction depths, provided a constant dopant concentration in the diffusant sol.

As previously shown, an inhomogeneous glass layer imposes a requirement for a thicker layer, in order to prevent built-in electric fields in the plane of the surface which increase recombination. Combined with the findings above, this means that the optimal lifetime resulting from deposition with the Sprutus apparatus is achieved by minimizing the sol layer thickness, while ensuring that the layer is thick enough for the major part of the total electric field to be directed perpendicular on the surface.

Chapter 6

Conclusion

This study has examined the concept of front-surface field passivation of back-junction solar cells. The aim has been to obtain an understanding of the relation between dopant profiles and the potential solar cell efficiency through a consideration of simple in-diffused silicon structures.

The results have shown that in order to obtain an efficient front surface field, relatively high values of sheet resistance are needed. A condition which must be satisfied for this to be valid is the depostition of a passivating layer on the silicon surface.

The simulation has also involved the comparison between two methods for determination of effective lifetime for photoconductance data. The study showed that the quasi-steady-state photoconductance method imposes a requirement of sufficiently long flash decays for correct results, which can not be met by the limited data set yielded from PC1D simulations. In the implementation of photoconductance results into the software for lifetime calculations, the photoconductance decay method is suitable and can be expected to yield results for all excess carrier densities.

The depth of the in-diffused p-n junction has been altered in the experimental work, seeking to optimize the effective lifetime and hence the potential efficiency of a back-junction solar cell. The findings have shown that with this method, the lifetime in theory will decrease with increasing junction depth for all nonzero depths. Assuming an ideally homogeneous in-diffusion of dopants, using a junction depth which is as low as possible yields the optimal dopant profile for a given peak dopant concentration. In practice, the diffused layer will exhibit inhomogeneities; using the peak dopant concentration as the varying parameter is then a more adequate method of optimizing the effecting lifetime.

Chapter 7

Future prospect

Several aspects regarding the back-junction technology have been left out in this work. An important issue is the mutual dependence of the process steps from wafer to the functional back-junction solar cell. For example, the utilization of high temperatures e.g. for oxidation may cause additional in-diffusion. The possibility of performing different processes simultaneously in one step is another important issue, in which there are many potential solutions. One example is the in-diffusion for the front surface field which may be combined with the creation of emitter regions on the rear side of the cell.

The phosphorus concentration in the P509 sol was a constant parameter throughout the experimental work. The results which have been presented indicate that a better means of optimizing the effective lifetime would be achieved by using the dopant concentration of the sol as parameter variable. As has been shown, however, the high viscosity of the sol causes large variations in spraying properties depending on the dilution ratio. An attempt to vary the phosphorus concentration therefore requires that the spraying method is substituted with spin-on deposition or that other measures are taken to ensure a controlled deposition process. For example, a thin layer of oxide or nitride may be grown on the surface under controlled conditions to act as a diffusion barrier for the phosphorus. Varying the thickness of the diffusion barrier may yield various peak concentrations.

Chapter 8

Appendix

A data sheet from the product catalog of spin-on diffusants from Filmtronics Inc. is shown in Fig. 1. The table displays in the range of phosphorus and boron spin-on dopant products manufactured by the company.

Figs.2 (a) and (b) display additional SEM results to the images supplied in section 5.1.3. In these images the thickness is approximately 2.0 μm on an average.

Fig. 3 shows the sheet resistance simulations obtained in Athena when temperatures from 700 °C are used. This plot is thus a prolongation of the simulation results in fig. 5.7 and was used to add sheet resistance values to Fig. 5.14.

The source code for Athena simulations is given below.

```
go athena

line  x loc=0         spacing=0.002
line  x loc=0.2       spacing=0.002
line  y loc=0       spacing=0.005
line  y loc=2         spacing=0.1

init silicon c.boron=3.5e15 orientation=100

impurity i.phos oxide dix.0=0.5 dix.e=3.1

deposit oxide thick=0.5 c.phos=4e20 divisions=500

method two.dim high.conc compress grid.ox=.01
```

```
diff time=25 temp=750 F.O2=21 F.N2=78.5 F.H2O=0.5

structure outf=oxide.str

etch oxide

extract name="xj" xj silicon mat.occno=1 x.val=0.0 junc.occno=1

extract name="rho" sheet.res material="Silicon" mat.occno=1
x.val=0.4 region.occno=1

structure outf=after_oxide_removal_1.str


# (Repeated 4 times with various diffusion temperatures)


tonyplot -overlay after_oxide_removal_1.str after_oxide_removal_2.str
after_oxide_removal_3.str after_oxide_removal_4.str
after_oxide_removal_5.str -set advdifex06.set

quit
```

PRODUCT DESCRIPTION
PHOSPORHOUS FILM P-500 TO P-509
BORON FILM B-150 TO B-155

B-150-155 and P500-509 yield doped layers on the silicon substrate upon drying. Advantages are improved yields, high purity, consistent coating, no problems with boron or phosphorous source wafers sticking to boats and no storage of source wafers. These solutions are high purity solutions from which boron and phosphorous may be diffused into silicon with little or no surface damage. These solutions have a shelf life of greater than 3 months at room temperature, longer times with refrigerated storage between 32°F and 40°F. The boron SOD's may also be used as an etch stop.

The surface concentrations observed upon post diffusion are a function of the concentration of dopant in SiO_2 film. The following concentrations are available:

	% Dopant Compound	$\%SiO_2$		% Dopant Compound	$\%SiO_2$
B150*	0.40	5.0	**P500**	0.06	8.0
B151*	1.00	5.0	**P501**	0.20	8.0
B152*	1.50	5.0	**P502**	0.24	8.0
B153*	2.00	5.0	**P503**	0.30	8.0
B154*	3.80	0.0	**P504**	0.50	8.0
B155*	4.00	0.0	**P505**	1.00	6.0
			P506	3.00	6.0
			P507	4.00	4.0
			P508	8.00	5.0
			P509	10.50	5.0

* Boron solutions B150 through B155 are unaffected by low humidity during application and subsequent processing

Application of dopant to silicon involves spinning at 2000 to 6000 rpm to produce an oxide looking film. Dopant would wet out uniformly over the surface of the silicon. If not, it will be necessary to produce a suitable hydrophilic surface for dopant to wet. This is accomplished by soaking the wafer in NH_4OH/H_2O_2 or H_2SO_4 – H2O2 solutions with rinses to render a suitable surface. After dopants are spun on, the wafer is heated to 200°C for 10-15 minutes to harden the film. These solutions contain ethyl alcohol as a solvent and may be thinned with ethanol or isopropanol to modify concentrations.

These solutions of boron and phosphorous should be applied using a polypropylene or delrin chuck for spinning. Approximately 1.0 ml or less is needed for a 2 inch slice or about 2.0 ml fir a 4 inch slice. After prebake, wafers may then be placed into the diffusion boat. A quartz "V" boat or oxidation boat with 0.1 inch spacing works well. Wafers should be placed perpendicular to the gas flow of the diffusion tube with 3 to 5 coated dummy slices at each end of the boat. Deviation in sheet resistance is reduced by placing coated sides facing each other.

Diffusion may be conducted from 900°C to 1300°C depending on process specifications in 90%N_2, 10% O_2 or other suitable ambient. Wafers are cleaned in HF after diffusion.

FILMTRONICS
SEMICONDUCTOR PROCESS MATERIALS

FILMTRONICS INC., BOX 1521, BUTLER PENNSYLVANIA 16003 U.S.A. • TEL: (724) 352-1772 • E-MAIL: SALES@FILMTRONICS.COM

Figure 1: Data sheet from the Filmtronics catalog, showing the phosphorus and SiO_2 content.

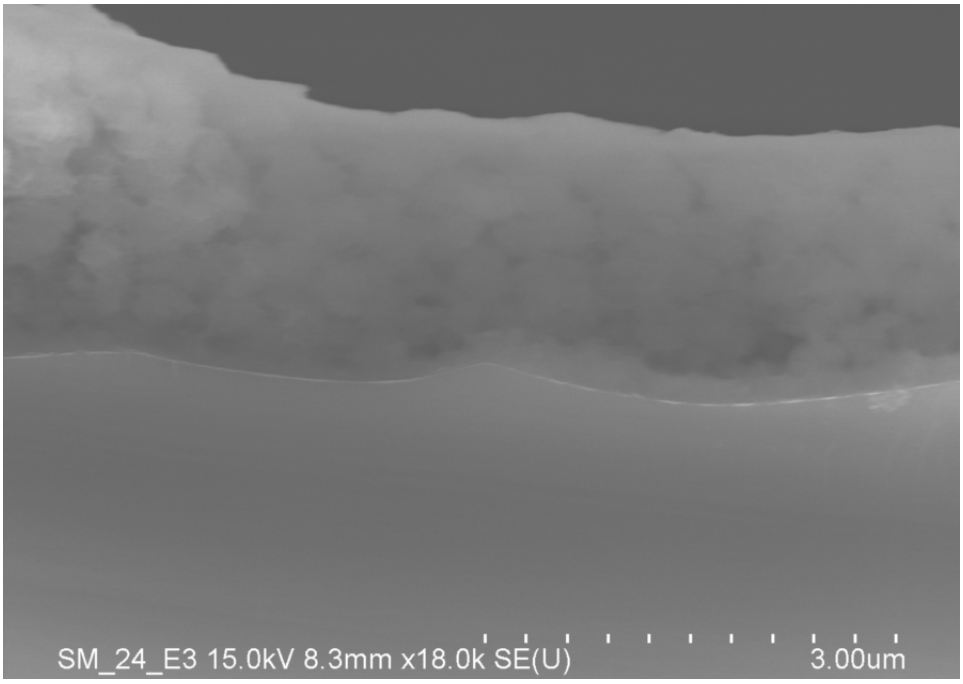

(a)

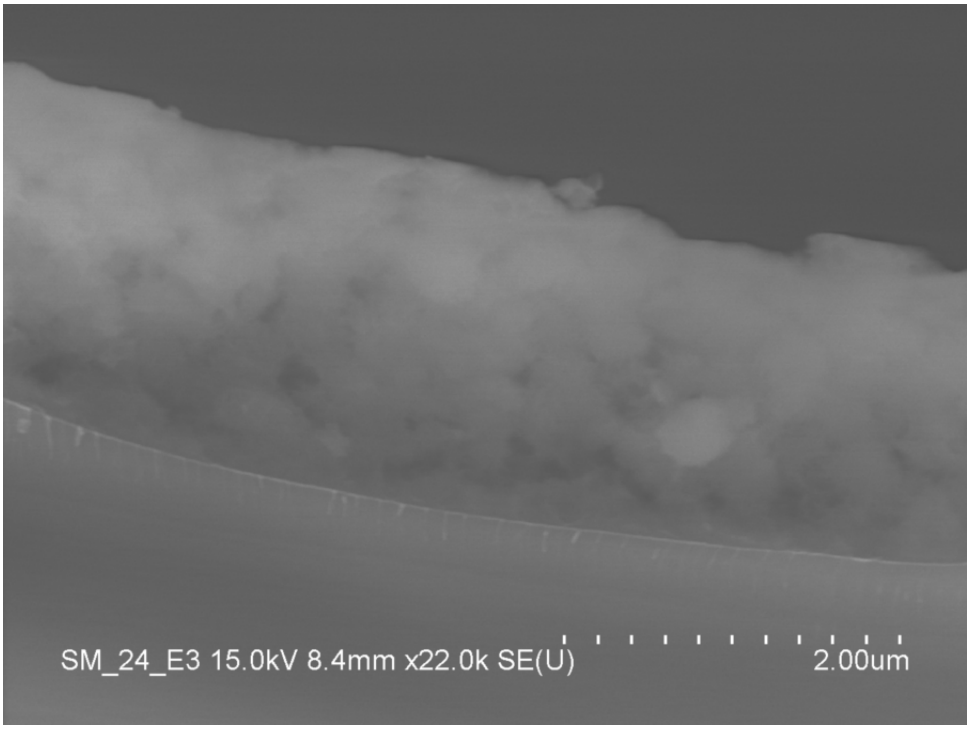

(b)

Figure 2: SEM images used for an indication of the oxide thickness in Athena simulations.

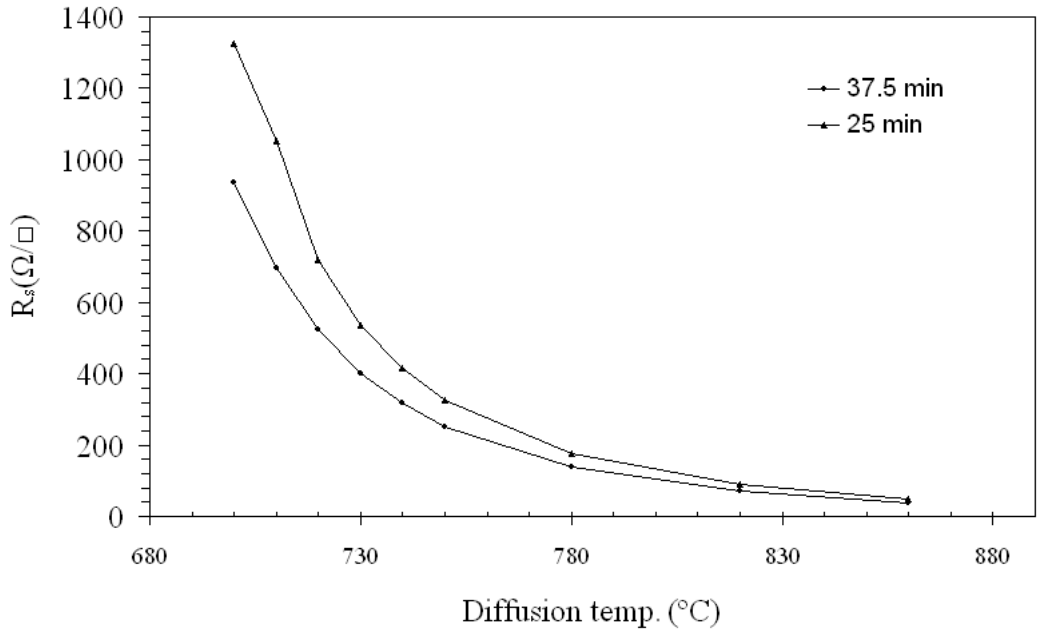

Figure 3: Simulations of sheet resistance as a function of diffusion temperature, where low temperatures are included.

Bibliography

[1] Boeker E and van Grondelle R. *Environmental Science - Physical Principles and Applications.* John Wiley & Sons, 2nd edition, 2001.

[2] Szweda R (ed). III-Vs: the power in space. *III-Vs Review*, 13:25, 2000.

[3] Lenardic D. Large-scale photovoltaic power plants: Cumulative and annual installed output capacity. *PVresources.com Annual Report*, 2007.

[4] Green A et al. Solar cell efficiency tables. *Prog. Photovolt: Res. Appl*, 16:61, 2008.

[5] Lammert MD and Schwartz RJ. The interdigitated back contact solar cell: a silicon solar cell for use in concentrated sunlight. *IEEE Transactions on Electron Devices*, 24:337, 1977.

[6] Nelson J. *The physics of solar cells.* Imperial College Press, 2003.

[7] Streetman BG and Banerjee SK. *Solid state electronic devices.* Prentice Hall, 6th edition, 2006.

[8] Aberle AG. *Crystalline silicon solar cells - Advanced surface passivation and analysis.* Centre for Photovoltaic Engineering, UNSW, 1999.

[9] Quirk M and Serda J. *Semiconductor manufacturing technology.* Prentice Hall, 2001.

[10] Campbell SA. *The science and engineering of microelectronic fabrication.* Oxford, 2nd edition, 2001.

[11] Neuhaus DH and Münzer A. Industrial silicon wafer solar cells. *Advances in optoelectronics*, 2007. ID 24521.

[12] Jester TL *et al. Grid-Competitive Residential and Commercial Fully Automated PV Systems Technology.* Proceedings of the 33rd IEEE Photovoltaic Specialists Conference, 2008.

[13] van Kerschaver E and Beaucarne G. Back-contact solar cells: a review. *Prog. Photovolt: Res. Appl*, 14:107, 2006.

[14] Dauwe S *et al. Very low surface recombination velocities on p- and n-type silicon wafers passivated with hydrogenated amorphous silicon films.* Proceedings of the 29th IEEE Photovoltaic Specialists Conference, 2002.

[15] Granek F *et al. Front surface passivation of n-type high-efficiency back-junction silicon solar cells using front surface field.* Proceedings of the 22nd European Photovoltaic Solar Energy Conference and Exhibition, 2007.

[16] Hench LL and West JK. The sol-gel process. *Chemical reviews*, 90:33, 1990.

[17] Sinton RA and Cuevas A. Contactless determination of current-voltage characteristics and minority-carrier lifetimes in semiconductors from quasi-steady-state photoconductance data. *Appl. Phys. Lett.*, 69:2510, 1996.

[18] Luque A and Hegedus S. *Handbook of Photovoltaic Science and Engineering.* John Wiley & Sons, 2003.

[19] Seth Burtner, Filmtronics Inc. E-mail correspondence.

[20] Toàn NN. *Spin-on glass materials and applications in advanced IC technologies.* PhD thesis, University of Twente, 1999.

[21] Basore PA and Clugston DA. PC1D, ver. 5.8. Software for one-dimensional simulations.

[22] Clugston DA and Basore PA. *32-bit solar cell modeling on personal computers.* Proceedings of the 26th IEEE Photovoltaic Specialists Conference, 1997.

[23] Nichiporuk O et al. Optimisation of interdigitated back contact solar cells by two-dimensional numerical solution. *Solar energy materials & solar cells*, 86:517, 2005.

[24] Mulligan WP *et al. Manufacture of solar cells with 21% efficiency.* Proceedings of the 19th European Photovoltaic Solar Energy Conference, 2004.

[25] Granek F *et al. Positive effects of front surface field in high-efficiency back-contact back-junction n-type silicon solar cells.* Proceedings of the 33rd IEEE Photovoltaic Specialists Conference, 2008.